INFERENTIAL MODELS FOR COMBUSTION PROCESSES

INFERENTIAL LATENT VARIABLE MODELS FOR COMBUSTION PROCESSES

by

Marlene Cardin, B.Sc (Eng)

A Thesis

Submitted to the School of Graduate Studies

in Partial Fulfillment of the Requirements

for the Degree

Master of Applied Science

McMaster University

MASTER OF APPLIED SCIENCE (2009)   McMaster University

(Chemical Engineering)   Hamilton, Ontario, Canada

TITLE: Inferential Latent Variable Models for

Combustion Processes

AUTHOR: Marlene Cardin, B.Sc(Eng)

(McMaster Unversity, Canada)

SUPERVISOR: Dr. John F. MacGregor

NUMBER OF PAGES: xiv, 95

ABSTRACT

This thesis investigates the application of latent variable methods to three combustion processes. Multivariate analysis of flame images and process data is performed to predict important quality parameters and monitor flame stability. The motivation behind this work is to decrease operational costs and greenhouse gases in these energy intensive processes. The three combustion processes studied are a lime kiln, a basic oxygen furnace and a coal-fired boiler.

In lime kiln operation, the main goal is to stabilize final product temperature in order to reduce fouling and energy costs. Due to long process dynamics, prediction of product temperature is required at least one hour in advance for potential use in a control scheme. Several methods for extracting features from flame images were investigated for the prediction of the temperature. The best method is then combined with process data in a PLS model that also incorporates dynamic information. The analysis revealed that prediction one hour into the future is successful using latent variable methods.

In the basic oxygen furnace analysis, the main goal is to predict end-point carbon of the batch process. Termination of the batch as soon as the desired carbon is attained reduces oxygen consumption and thus operational cost. Traditional image analysis is used to identify a constant field of view in the flame images. Multivariate image feature extraction methods were then used in combination with process data to successfully predict the final carbon content of the heat.

The coal-fired boiler analysis focuses on monitoring of flame stability at different production and air to fuel levels of the boiler. Prediction of energy efficiency and off-gas chemistry from flame images is also investigated. An unexpected result was the ability to use the installed cameras for localized fouling monitoring.

This thesis showed that the use of multivariate analysis of flame images and process data in combustion process is very promising.

ACKNOWLEDGEMENTS

Table of Contents

List of Figures

List of Tables

Chapter 1

Introduction

Motivation and Goals

In recent years, Canada's manufacturing industry has been struggling financially with increased energy costs and a high Canadian dollar. Additionally, more stringent environmental regulations have been enforced to decrease greenhouse gas emissions. Research into improving energy efficiency and using alternate fuel sources in combustion processes has been sparked by these challenges and motivates the work presented in this thesis.

The goal of this research it to apply latent variable methods to several combustion processes to provide process stability, predict product quality and improve energy efficiency. The methodology used combines flame images and process data in a multivariate analysis to monitor and control three different processes. A lime kiln in the pulp and paper industry, a basic oxygen furnace in the steel industry, and a coal-fired boiler for power generation are studied in this work. An overview of the key goals of each analysis is provided.

Lime Kiln

A rotary lime kiln is a continuous recycling process used in pulp and paper mills. It converts calcium carbonate into lime for reuse in the pulp process. The reaction requires high temperatures and long exposure times, leading to slow process dynamics. As a result,

1

operators have difficulty controlling the product temperature. Fouling is increased with temperature fluctuations and can lead to unscheduled shutdowns and costly maintenance. Temperature fluctuations also lead to suboptimal conversion of calcium carbonate to lime. The main goals are to use the data to predict product temperature several hours in advance, for potential use in a control scheme. An increase in energy efficiency and reduction in fouling will lead to significant cost and greenhouse gas reductions.

Basic Oxygen Furnace

A basic oxygen furnace is a batch process used in steel mills to produce refined steel. Oxygen is injected into a bath of molten iron and scrap metal to remove carbon and other impurities. In this thesis an analysis is performed to predict end-point carbon content, which is the main measurements for batch termination. Knowledge of when to terminate the batch is key to producing high quality steel with minimum energy and oxygen requirements.

Coal-fired boiler

Coal-fired boilers are used to generate superheated steam that is transferred into electricity. However, they are significant greenhouse gas producers and are no longer an attractive method for energy production. A combined research team, funded by the Canadian Government, is investigating conversion of a coal-fired boiler to a biomass fed boiler. McMaster University's involvement in this team encompasses using flame images and process data for monitoring of flame stability, energy efficiency and fuel stability.

Thesis overview

Chapter 2 – Literature Review and Discussion of Methods

A discussion of key latent variable methods (PCA and PLS), handling of missing data, and multivariate image analysis is presented. Differences between multivariate analysis for batch and continuous processes are explained.

Chapter 3 – Lime Kiln Analysis

This chapter presents the results of the lime kiln data analysis beginning with a description of the process and available data. Predicting product temperature using several image feature extraction methods is detailed. Incorporating dynamics into image only and PLS models combining images and process data is discussed.

Chapter 4 – Basic Oxygen Furnace Analysis

The results of the basic oxygen furnace analysis are presented in this chapter. Image pre-processing is required in this analysis and is presented as well as the various types of image feature extraction methods investigated to predict end-point product quality. The preliminary results of a model combining both the images and process data are shown.

Chapter 5 – Coal Fired Boiler Analysis

This chapter presents the results of the studies performed at the Atikokan power generation station. A designed experiment of the boiler operating at different production rates and air to fuel ratios was completed to determine whether process and image data could identify the various operating conditions. The results of the image analysis of these coal-only experiments are presented herein.

Chapter 6 – Conclusions and Recommendations

Key results obtained in this thesis are summarized in this chapter. Recommendations for future work are detailed.

Chapter 2

Background and Discussion of Methods

This chapter presents an overview of the methods used in this research.

2.1   Background

Statistics have been used in monitoring and process control for several decades, most commonly through the use of statistical process control charts (SPC). Increased instrumentation and data historizing has led to exponential growth in available data to analyze processes. Monitoring and analyzing such a large dataset one variable at a time is time-consuming and often ineffective. This has given rise to the use of multivariate statistical methods in process troubleshooting, monitoring and control. These methods can effectively handle several of the key concerns with process data: high dimension, collinear measurements, noise and missing data (Eriksson *et al.* [2006]). Through the use of principal component analysis (PCA) or partial least squares (PLS) a system can be reduced to a few key latent variables, that can then be used for troubleshooting, monitoring and control. Industrial use and applications of these methods have risen in recent years. For example, ArcelorMittal

Dofasco, a steel company located in Hamilton, Ontario, has successfully used these methods for several years. Offline data analysis is performed regularly, as well as online control of their desulpherization process using a PLS model, and castor breakout monitoring using a PCA model (Dudzic and Quinn [2002]:Dudzic et al. [1999]).

A natural extension of the multivariate data analysis approaches are to colour image analysis, where the images are large in size and the three colour channels, RGB, are highly correlated. Colour cameras are inexpensive sensors that are often installed to aid the operators in monitoring processes from the control room. Information from cameras is rarely tied into a database or control system. However, through the use of multivariate statistics, it is possible to efficiently extract relevant features from images for online monitoring and control. In the snack food industry multivariate colour image analysis is used to predict and control seasoning content of chips. (Yu and MacGregor [2003b]). In the lumber industry, a similar methodology was used to grade lumber quality, by identifying defects such as knots and splits. (Bharati and MacGregor [1998]).

In combustion processes cameras are commonly installed for operator viewing of the flame from inside the control room. Operators mainly use the camera to detect a major process instability, such as a complete lack of flame. However, much more information is contained within these images, and could be extracted using multivariate methods. A study of a waste boiler (Yu and MacGregor [2004]) and rotary ore roasting kiln (Szatvanyi and Duchesne [2006]) have already been completed. In the waste boiler analysis, key features were extracted from flame images and combined with process measurements to predict important process parameters such as off-gas concentrations and energy content of the waste fuel stream. These are difficult and expensive to measure, therefor, obtaining accurate predictions from image and process data is a significant achievement. The success of this boiler analysis sparked the interest in the rotary ore roasting kiln analysis. This study showed promise for prediction of final solids temperature several hours into the future. This prediction into the future is important as the process has long dynamics, and the operators have difficulty maintaining a stable temperature. Unfortunately, neither of these two studies led to an online implementation, and the area of flame image analysis is currently an active

development area.

2.2 Multivariate Analysis Methods

Multivariate analysis approaches are successfully used for analysis of process and image data because of their ability to handle missing data, noise, collinear measurements and large amounts of data. This section presents a description of the multivariate methods used in this work, including principal component analysis, partial least squares, and calculation with missing data.

2.2.1 Principal Component Analysis

Principal component analysis is an important multivariate statistical tool that is utilized to determine the directions (latent variables) of largest variability in a given set of measurements. Usually only a few latent variables explain can explain most of the variance in a highly correlated data set such as a set of process measurements or images. PCA is well documented in many literature sources (MacGregor and Kourti [1999] : Eriksson *et al.* [2006]) thus only a brief description is provided here. The model is in the from of:

$$X = TP^T + E \tag{2.1}$$

where:

- X is the original data matrix (nxk)

- T is the latent variable score matrix (nxA)

- P is the loading matrix (kxA)

- E is the error matrix, or noise (nxk)

- A is the number of latent variables (components) in the model

- n is the number of observations

- k is the number of variables in the dataset

The first column of the loading matrix (1st component, P_1) represents the direction of greatest variance of the observation in X. This is calculated as the largest eigenvector of the covariance matrix, $X^T X$, and is normalized to unit length. The second loading vector, P_2, represents the second greatest direction of variance in the observations of X, with P_2 being orthogonal to P_1. Figure 2.1, adapted from ProSensus Inc. [2007], shows two components of a dataset. The scores (T) are the coordinates of each observation in the coordinates of P.
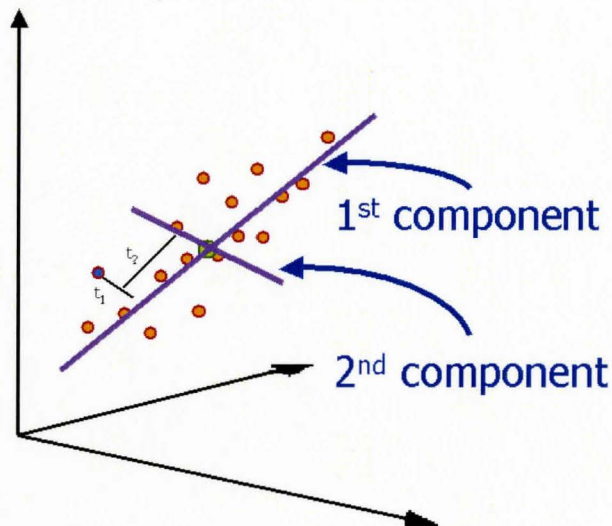
Figure 2.1: Illustration of PCA (ProSensus Inc. [2007])

The number of components used to fit a dataset should be such that no random noise is modeled. A dataset is often split into training and testing data to ensure that the model for each dataset performs similarly. Another popular method is cross-validation, discussed in [Eriksson *et al.* [2006]]. The calculation of the components can be performed through the use of NIPALS (non-linear iterative partial least squares) algorithm (Kresta *et al.* [1994]:Geladi and Kowalski [1986]:Eriksson *et al.* [2006]). NIPALS algorithm is readily adapted for missing data, which is discussed in Section 2.2.3. Appendix A provides more detail on the NIPALS

algorithm.

Prior to building a PCA or PLS model, the data are normally mean centered and scaled to unit variance. Mean centering prevents the model from having to fit the average of each variable. Scaling each variable to unit variance is performed so that each variable has the same range. Without this step, a variable with a large range would be given more importance in the model since multivariate methods attempt to model the greatest sources of variance in a dataset. (Eriksson *et al.* [2006])

2.2.2 Partial Least Squares

Partial least squares (PLS), is very similar to PCA, however, in this case there exists a set of prediction variables (Y) as well as the set of process measurements (X). A model is fit so that the maximum variance in both data sets is explained as well as the correlation between the two. This represents a large advantage over traditional regression methods, because both the X and Y space are modeled. PLS is well documented in literature sources (MacGregor and Kourti [1999] : Eriksson *et al.* [2006]: Kresta *et al.* [1994]), and will only be briefly described here. The model is in the form of:

$$X = TP^T + E \tag{2.2}$$

$$Y = UC + F \tag{2.3}$$

$$T = XW \tag{2.4}$$

where (additional variables not described in PCA):

- Y is the quality data matrix (nxm)

- C is the Y loading vector (mxA)

- U is the Y space score

- F is the error matrix of Y (nxm)

The first latent vector, W_1, is the largest eigenvector of the covariance matrix X^TYY^TX, normalized to unit length. For the second latent vector, the X space is deflated so that X is orthogonal to T_1, and the largest normalized eigenvector of the new covariance matrix is W_2. This continues until all the desired components are calculated. The X and Y space are linked by U=T, and the Y loading vector,C, is determined by a least squares projection shown in equation 2.3. These steps ensure that the maximum variance of both the X and Y datasets are explained, as well as the correlation between the two. An illustration is provided in Figure 2.2, adapted from ProSensus Inc. [2007].
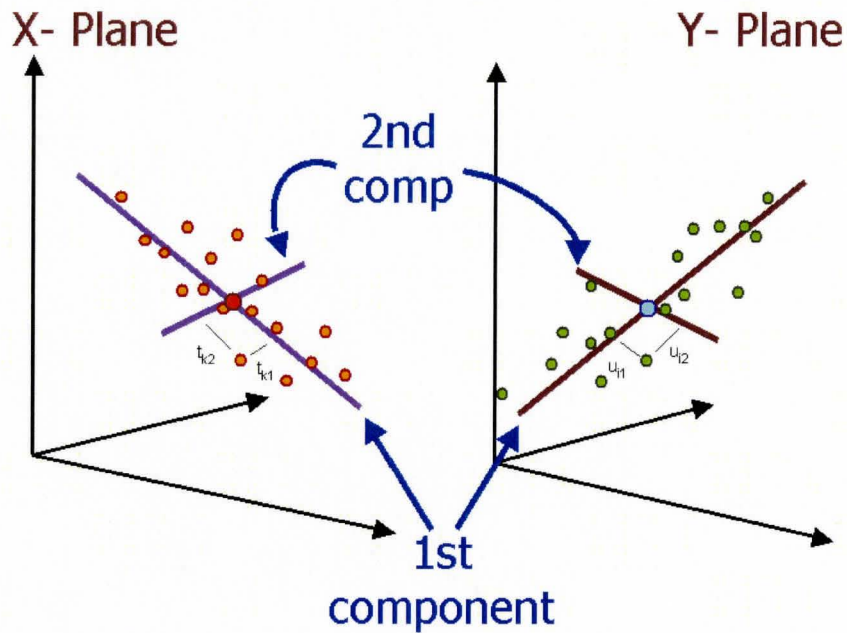
Figure 2.2: Illustration of PLS(ProSensus Inc. [2007])

As with PCA, the loading vectors can be calculated through the use of NIPALS algorithm (Kresta *et al.* [1994]:Geladi and Kowalski [1986]:Eriksson *et al.* [2006]), shown in Appendix A. The number of components that are used are again determined by cross-validation (Eriksson *et al.* [2006]), to avoid over-fitting of the data.

2.2.3 Handling Missing Data

The ability to handle missing data is essential when dealing with process measurements. Data are missing from process historians if sensors fail or if different sampling rates exist amongst the measurements. There are various methods described in literature to handle missing data, with varying degrees of complexity and accuracy (Nelson *et al.* [1996] : Arteaga and Ferrer [2002]). Depending on whether or not data are likely to fail in blocks (i.e., a whole group of process measurements fails at once) or just one variable at a time, different approaches can be used. For the scope of this work, it is anticipated that process measurements would not fail in blocks, and that the amount of missing data is minimal. If the camera would fail, the entire block of image features would be missing. Since the image features are extremely important for accurate prediction, no model calculation would be performed if this failure were to occur. The only time a prediction would be required with missing data present is when just a few process measurements have failed. The simplest method, single component projection (SCP) is used. This approach is based on the NIPALS algorithm, where a model is built that ignores any data that is missing(Nelson *et al.* [1996]). This is incorporated into the NIPALS algorithm shown in Appendix A for both PLS and PCA modeling. With a new observation, the scores are calculated by ignoring missing data, one component at a time, by the following set of equations (Nelson *et al.* [1996]):

$$T_\alpha = P_\alpha^{*T} X(\alpha)^* / P_\alpha^{*T} P_\alpha^* \tag{2.5}$$

$$X(\alpha + 1)^* = X(\alpha)^* - T_\alpha P_\alpha^* \tag{2.6}$$

where:

- alpha represents the component being calculated

- * indicates only the loadings for which the data is present

The set of equations shown above is for a PCA model. If the model is a PLS model, P* is replaced by W*.

2.3 Multivariate Image Analysis

This section presents the steps required for multivariate image analysis (MIA), model building and some image feature extraction techniques. Further details can be found in literature sources (Bharati and MacGregor [1998] :

Step 1: Image Decomposition

A colour image consists of a red, green and blue channel. Each channel is an MxN matrix, consisting of entries between 0 and 255. Various combinations of the entries in the three channels lead to different visual colours in an image (for example, R=255, G=255, and B=255 is a white pixel). Therefor, the resulting image matrix has dimension MxNx3, as shown in Figure 2.3. In order to perform a PCA on the data, the image must first be decomposed to a (mxn) *3 vector, as presented in Figure 2.3
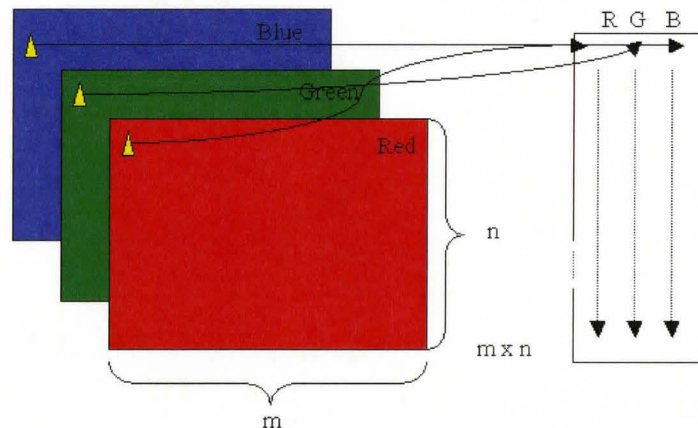
Figure 2.3: Image Decomposition

Step 2: Image model calculation

In order to determine the image model,the overall covariance matrix, X^TX, image is calculated (X being the decomposed image). Where there is more than one image, the sum of the X^TX matrices for all of the images is used. Singular value decomposition is then performed on this matrix to obtain the loading vector,P. A 2 component PCA model is normally used, since there are only three variables (red, green, and blue) in an image. The channels are

so highly correlated that the first component often explains more than 95 percent of the variation in the image matrix.

Step 3: Calculate scores and show as image

The scores are calculated by the following formula (Yu and MacGregor [2003a]):

$$T = X * P^T \tag{2.7}$$

In order to view the scores as an image, the scores are scaled and re-folded into a 256 by 256 histogram image. The scores are scaled using the minimum and maximum score for each component, over all of the images in the training set. The scores are then scaled between 0 and 255 (the range of RGB pixels) by the following formula (Yu and MacGregor [2003a]):

$$Tscaled_{k,i} = round\left(\frac{t_{k,i} - t_{k,min}}{t_{k,max} - t_{k,min}} * 255\right) \tag{2.8}$$

- k is the component

- i is the pixel

- Tscaled is the scaled score value

- $t_{k,max}$ is maximum score value at component k

- $t_{k,min}$ is minimum score value at component k

A histogram image is then created using 256 bins in both the T_1 and T_2 components. 256 bins are used because there are 256 possible values that the scaled scores can have (between 0 and 255). The image is color coded to present bins with high pixel counts as bright spots, and bins with low pixel counts as black spots. Figure 2.4 presents an image from the lime kiln and the respective score image.

Step 4: Extracting Features from the score plot

Extracting features, or characteristics, from the score histogram is the most important step
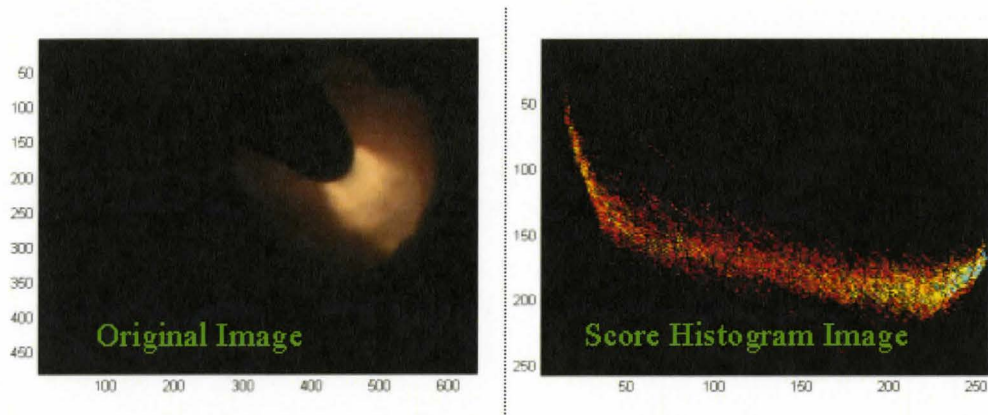
Figure 2.4: Original Image and Score Histogram of a kiln image

for creating successful models. The reason is that these features are combined with process data to create PCA or PLS models for prediction, monitoring and control. If the features are inadequate, the model will be less accurate. This extraction step varies from application to application as different image features are important for any given model. Two of the most common feature extraction methods include using masks (counting the number of pixels falling into a certain area of the score plot) or using all the bins from the score histogram in the model. The use of a mask on a lime kiln image is illustrated by Figure 2.5. The number of pixels falling under that mask for every image is a new variable.

2.4   Batch and Continuous Processes

This thesis involves the study of a batch process and two continuous processes. A batch process is operated until a certain objective is met, while a continuous process is operated ceaselessly. Batch processes require data pre-processing before a multivariate analysis can be performed because process measurements vary with time. This creates a three dimensional matrix, that must be decomposed as shown in Figure 2.6 (ProSensus Inc. [2007]). It is possible that the data must also be aligned before they are in a format with which PCA
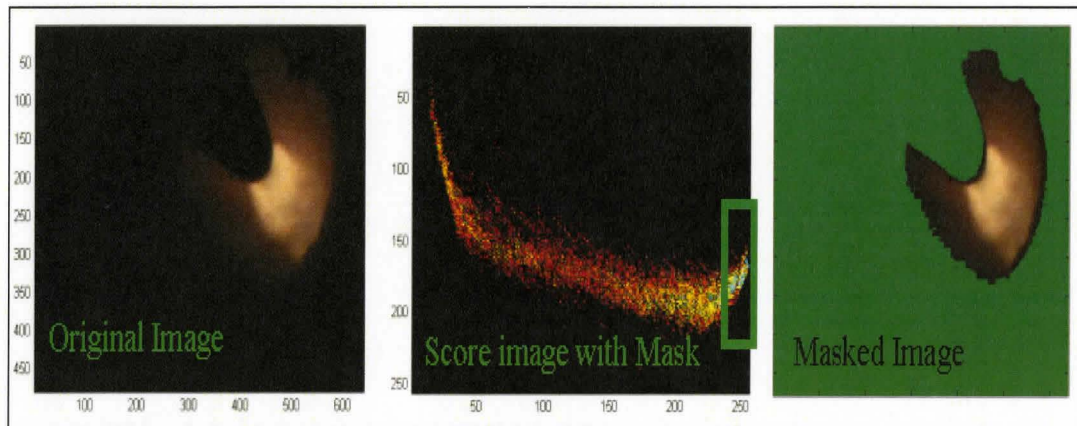
Figure 2.5: Demonstration of feature extraction using masks on a kiln image

and PLS models can be created. This step is required if the batches are not of the same duration or if an indicator variable is present that better describes the progression of a batch. Further reading on batch processes and alignment can be found in [Nomikos and MacGregor [1994]:Westerhuis *et al.* [1999] and Kassidas and MacGregor [1998]). The alignment required for the batch process studied in this work will be discussed in greater detail in the Chapter 4.
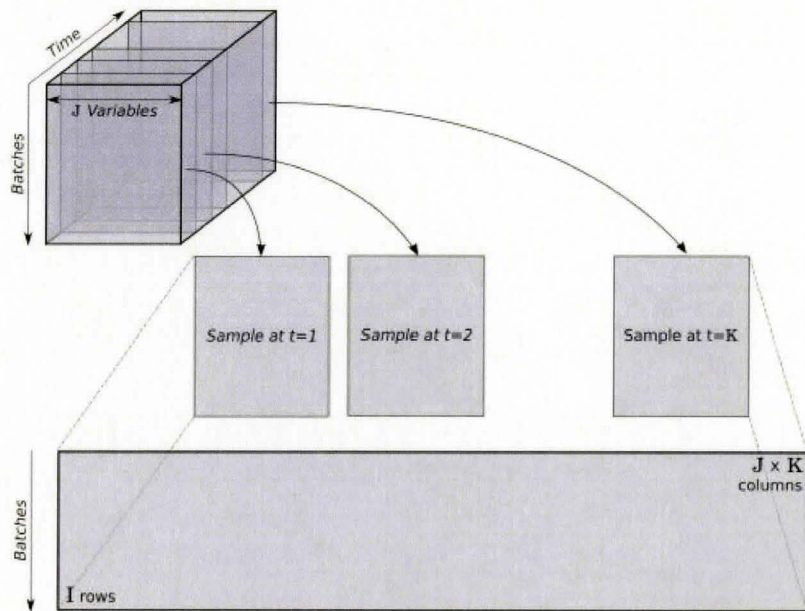
Figure 2.6: Decomposition of batch data (ProSensus Inc. [2007])

2.5 Programs Used

The following is a list of the various programs used in this work:

- MATLAB R2007b : for data pre-processing, analysis and model building

- Umetrics Simca-P+ 11.5 : for multivariate model building

- MACCMIA : for preliminary multivariate image analysis

Chapter 3

Lime Kiln Analysis

3.1 Introduction

Rotary kilns were first introduced in the late 1800's to be used as reactors or driers for several different types of raw materials. Although they are most commonly used for cement and lime production, ore roasting and refractory production is also preformed in kilns. (Boateng [2008] : Szatvanyi and Duchesne [2006]). Regardless of the purpose of a rotary kiln, they face similar operational challenges including fouling, inefficient operation, greenhouse gas emissions and high energy costs. Inefficient operation and fouling is mainly caused by inadequate temperature control, which occurs due to long process dynamics and variations in raw material quality. Fouling leads to expensive, unplanned maintenance outages for cleaning. Inefficient operation results in higher energy use, higher greenhouse gas emissions, and poor product quality. Recently, the use of alternative fuels in kilns has become attractive for green house gas and energy cost reduction. Unfotunatley, their use is often prevented by the inability to control temperature and stabilize kiln flames. This chapter addresses these challenges using multivariate analysis of flame images and process data of a lime kiln.

The rotary lime kiln studied in this chapter is a brand new installation at Irving Pulp and Paper (IPP) 's Saint John, New Brunswick. This unit is required for conversion of $CaCO_3$

(called mud) to CaO (lime) for reuse in the paper making process. This kiln was built to replace two older, small kilns and the entire plant is now shutdown when an outage is required to clean the fouled kiln. Operators have difficulty manually controlling this new, larger kiln, which has resulted in several process upsets over the first 8 months of operation. Figure 3.1 shows the clean and the fouled kiln that occurred after only a few months of operation. For obvious reasons, the fouling is often referred to as ringing. Reducing and controlling fouling, product temperature and product chemistry are critical and will be the main focus of this work. Refer to Appendix C for a flow sheet of a kraft pulp and paper mill such as this one.
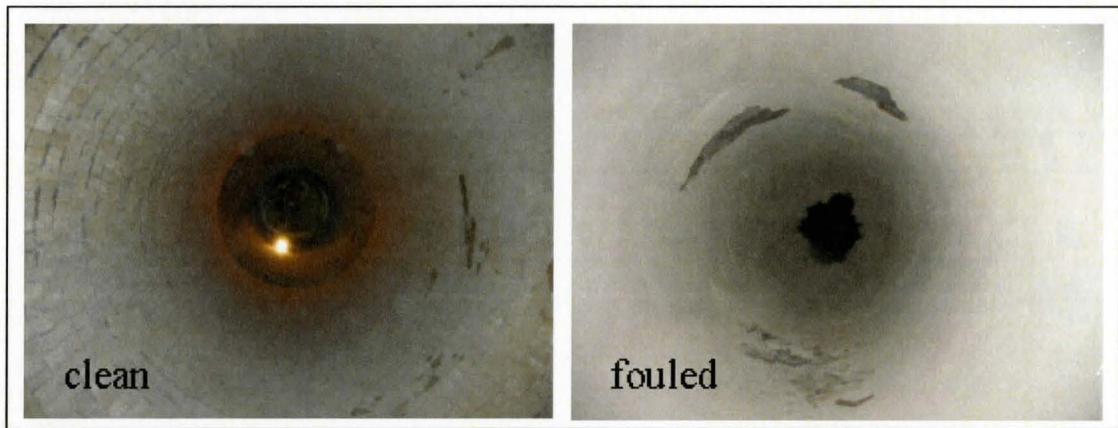
Figure 3.1: The Irving Pulp and Paper kiln clean and fouled

Rotary kilns are all of similar design. As shown in Figure 3.2, material and gas flows are counter-current, and the kiln is on an angle to gradually allow the raw material to pass through the kiln. The kiln is rotated to improve mixing and increase throughput (Boateng [2008]). The IPP lime kiln studied in this work uses oil as the fuel source. Manual control of the exit gas temperature, product chemistry and product temperature is performed by manipulating air and fuel flows. The incoming material, mud, is varied based on upstream demand for lime. Figure 3.2 also depicts some of these important temperature and flows (described in more detail in Section 3.2.2).
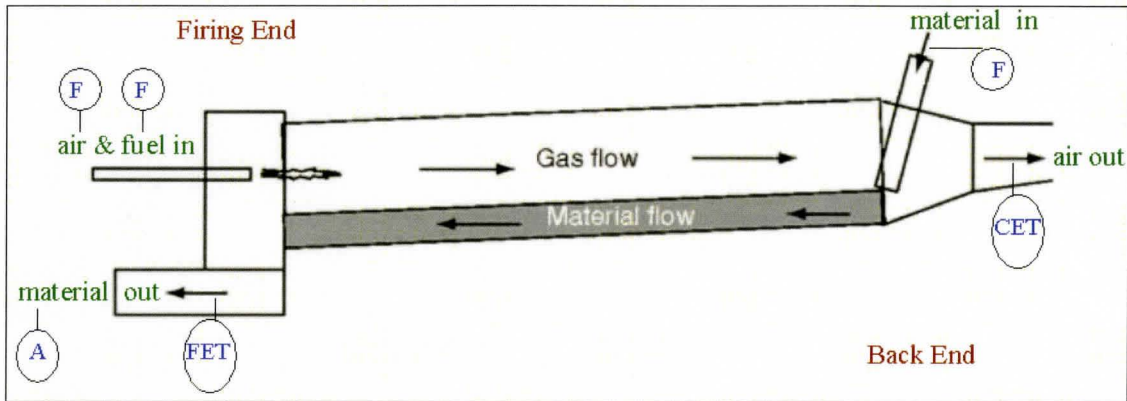
Figure 3.2: Rotary kiln diagram(Boateng [2008])

3.2 Data Available and Experiments Performed

Now that the main process has been explained, this section will provide an overview of the process and image data available at the IPP kiln, as well as the experiments that were performed on site.

3.2.1 Vision System

High temperature cameras are implemented at some kilns for operator flame monitoring. Being brand new, the IPP kiln was outfitted with a cutting edge, air cooled, digital camera with seamless recording capability. The camera is a Quadtek Spyrometer[3] M554 (Quadtek Mirion [2008]). As can be seen in Figure 3.3, the camera is located at the firing end of the kiln, with a clear view of the flame. This ready availability of good quality image data greatly facilitated the project.

3.2.2 Process Data

There are various process measurements available on a modern kiln. For this analysis, the measurements are divided into manipulated variables, response (controlled) variables and
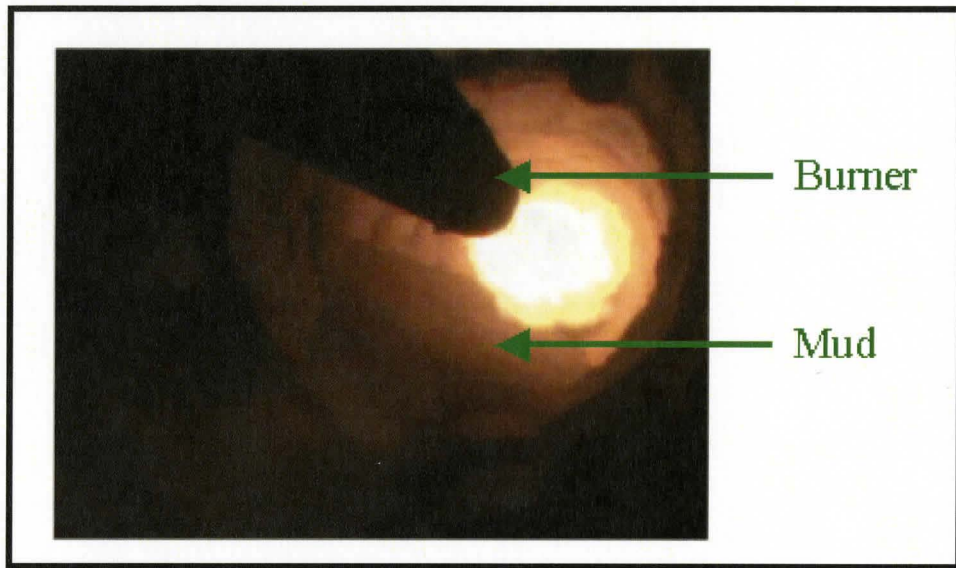
Figure 3.3: Typical image from Irving Pulp and Paper's kiln camera

other process measurements.

Manipulated Variables:

- Mud flow , oil flow and air flow

Response Variables:

- Firing end temperature (FET): the final product temperature

- Cyclone exit temperature (CET): the temperature of the air exiting the cyclone (at the back end of the kiln)

- Residual $CaCO_3$: a lab measurement of the amount of $CaCO_3$ remaining in the produced lime

Other process measurements

- Off-gas chemistry (oxygen, carbon monoxide, hydrogen sulfide, etc)

- Back-end temperature and pressure

- Kiln rotational speed, voltages and motor amps

- Surrounding equipment(precipitator, filters, vacuum) temperature and pressures

3.2.3   Experiments

Experiments were performed over a four day period in order to gather data at various operating conditions. With the completion of experiments, a rich dataset is generated in a short amount of time. This is beneficial because image data are computationally intensive to analyze. Having 4 days of data from a designed test as opposed to several months of historical data reduces analysis time and provides more process information.

Detailed experiments were planned in a 2^3 design to manipulate air, mud and oil flow. The manipulated variable set points were carefully selected to keep the firing end temperature within quality specifications. Upon discussion with operating personnel some experiments were removed because the cyclone exit temperature would have exceeded safe operating conditions. Nonetheless, a large range of process conditions were operated and excellent data were obtained. Figures 3.4 and 3.5 present the manipulated and controlled variable values throughout the experiments. Note that the data were mean centered and scaled to unit variance for easy visualization. The images and process data were recorded every 10 seconds. Residual $CaCO_3$ lab tests were performed at 20 minute intervals instead of 2-3 hours intervals during regular operation.

3.3   Results and Discussion

The dataset obtained during process experiments was used for residual calcium carbonate prediction, process identification, temperature prediction using images and process data and a preliminary analysis of flame stability.
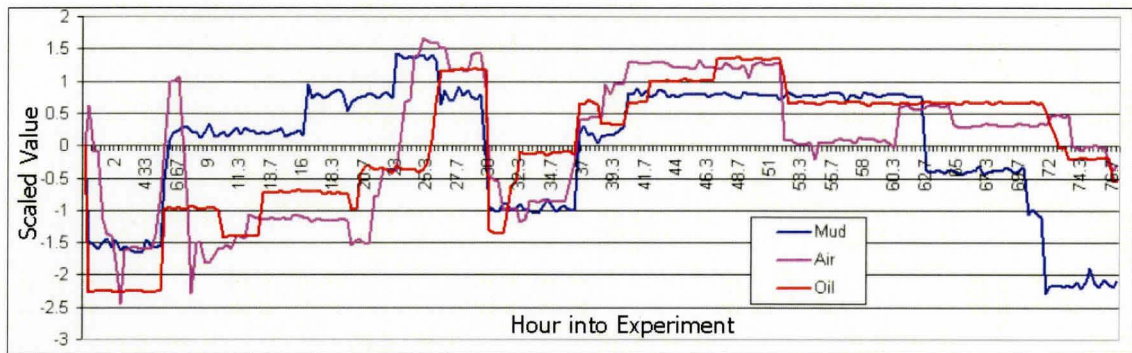
Figure 3.4: Time series plot of manipulated variable during experiments
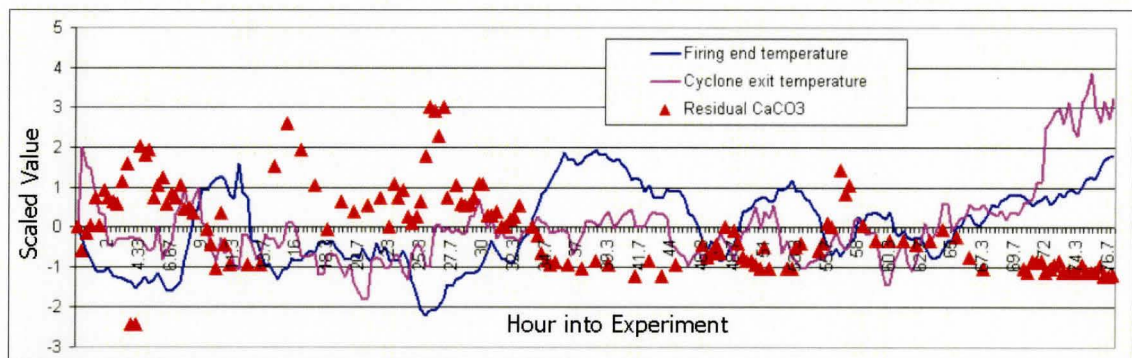
Figure 3.5: Time series plot of response variable during experiments

3.3.1 Residual Calcium Carbonate Prediction

The measure of the amount of $CaCO_3$ remaining in the lime is the main measure of product quality in the kiln. High $CaCO_3$ content indicates that the process was run inefficiently and the final lime contains significant impurity. The procedure to obtain this measurement contains several steps including taking a product sample, grinding sample, adding chemicals, taking a reading from a graduate cylinder, then reading the corresponding value of residual calcium carbonate off a graph. As a result, this measurement is time consuming and contains several sources of variation. One goal of this work is to create an accurate, online soft sensor to predict residual $CaCO_3$.

Throughout the experiments it was noted that firing end temperature (FET) and residual calcium carbonate are highly correlated, as shown in Figure 3.6. A linear correlation between the two measurements explains 68 percent of the variation in residual $CaCO_3$. Given the amount of variation in the quality measurement, it is unlikely that a more in depth analysis would provide an improvement in prediction. Since the residual calcium carbonate can be inferred from the firing end temperature, FET prediction several hours into the future becomes the main focus of this work. With a successful prediction of FET, control moves could be made to ensure stable FET, which would also stabilize and improve residual calcium carbonate.
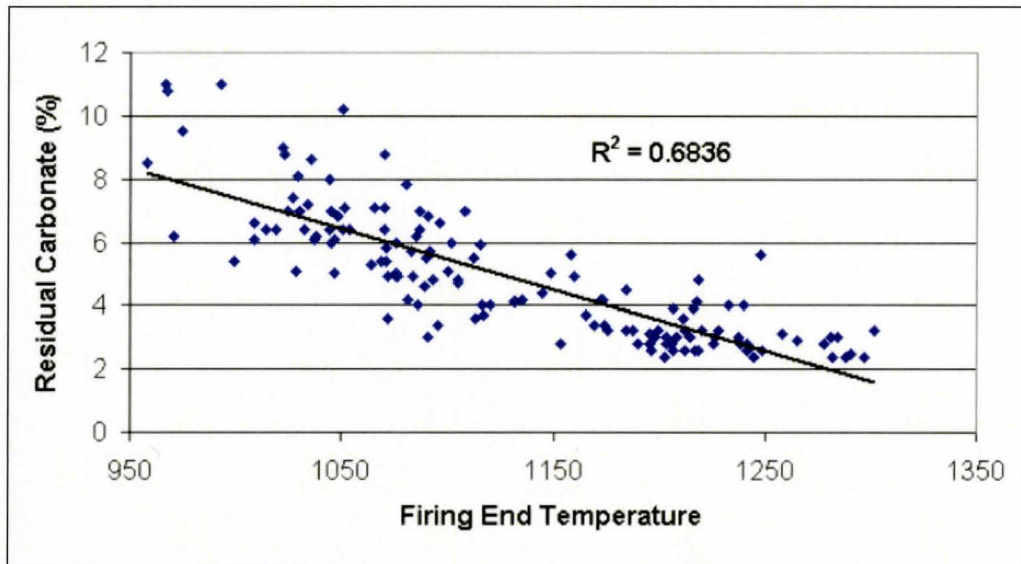
Figure 3.6: Correlation between Firing End Temperature and Residual Calcium Carbonate

3.3.2   Process Identification

It is important to characterize the dynamics between the manipulated and response variables for process understanding and for use in control algorithms. First-order with dead-time models were used to fit the data, which take the form: (Marlin [2000])

$$\Delta Y = \Delta MV * Kp_{MV} * (1 - exp(-(t - \theta_{MV})/\tau)) \qquad (3.1)$$

where:

- Y is the response variable

- MV is the manipulated variable

- Kp is the gain

- Θ is the dead-time

- τ is the time constant

The three parameters of equation 3.1; Kp, Θ and τ are calculated using the process reaction curve method described in [Marlin [2000]]. During the experiments, there was individual step changes made to one manipulated variables where the others were left constant, and from there, the parameters could be calculated. This occured around hour 49 for oil, hour 60 for air, and hour 63 for mud. The results of the identification for the three manipulated variables and two response variables are shown in Table 3.1. These parameters were verified with knowledge from process engineers to ensure they were accurate. Increasing air flow draws heat from the firing end of the kiln to the back end, thus cooling FET and increasing CET. Air also has a short time delay and the shortest time constant. An increase in the mud flow cools both temperatures, and has a faster impact on CET than the FET as it is charged at the back end of the kiln. An increase in oil flow increases energy to the process, thus increasing both temperatures.

3.3.3 Firing End Temperature prediction using image features

This section presents how FET is predicted using three methods of image feature selection. The method that generates the best results will be combined with process data to obtain a final model (Section 3.3.4). PLS models are created where the image features are used to predict temperature at the current time, 1 hour in advance and 2 hours in advance. The three methods of image feature selection studied are:

Table 3.1: Identified Process Parameters

Parameter	Unit	FET	CET
Gain,air	$\Delta\,^\circ F/\,\Delta$ RPM	-1.67	0.93
Gain,mud	$\Delta\,^\circ F/\,\Delta$ USGPM	-5.00	-1.55
Gain,oil	$\Delta\,^\circ F/\,\Delta$ USGPM	700	150
Time constant,air	minutes	22.60	5.8
Time constant,mud	minutes	67.85	10.73
Time constant,oil	minutes	62.50	50.00
Time delay,air	minutes	4.02	3.06
Time delay,mud	minutes	86.91	0.00
Time delay,oil	minutes	83.33	141.6

1. Average RGB Method

2. Cumulative Histogram Method

3. Mask Method

Average RGB Method

In combustion processes, production rates and temperatures are highly correlated to the image brightness. From each image, the average red, green and blue value is calculated as well as the difference between the colour channels (average red-average blue, average green-average blue, and average red-average green). A total of six features are obtained from each image and can be used to predict FET. The advantage of this method is that it is computationally simple and does not involve multivariate image analysis methods. However, it is likely that there are other features in the images that are not captured with the average colour that could enhance the FET prediction.

Cumulative Histogram Method

The cumulative histogram method involves calculating the score histograms over all of the images in the training set (as described in Section 2.3). Using this information the steps below are followed to obtain features from the images:

1. Reduction of the score histograms from 256 x 256 matrices to 32 x 32 matrices

2. Unfolding of the 32 x 32 score histograms to 1x 1024 vectors

3. Calculation of the cumulative sum vector of each 1 x 1024 vector

4. Combining the cumalitive sum vectors of all N training images into an N x 1024 matrix

5. Fitting an 8-component PCA model to the N x 1024 matrix

6. Use of the 8 scores of the PCA model as features of each image

Steps 1-3 are illustrated for one process image in Figure 3.7. This method captures more image characteristics than the RGB method, however, it is very difficult to relate the features back to the image for interpretation of results.
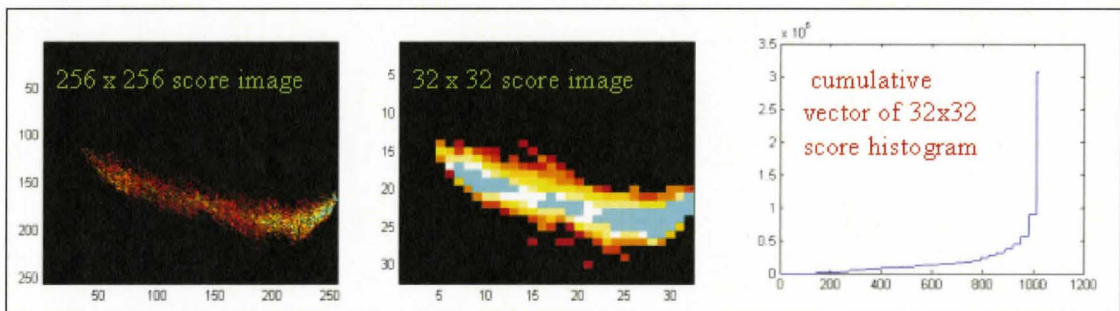
Figure 3.7: Steps 1-3 of the cumulative histogram feature extraction method

Mask Method

This method also requires the score histograms of all the images. 12 masks are applied to the score histograms and the number of pixels belonging to each mask are the features extracted from this method. A score histogram with the 12 masks applied to each histogram are shown in Figure 3.8. Figure 3.9 presents the regions of a kiln image to which each mask corresponds to. In this particular image there were no pixels that belonged to Mask 1 and 12. Mask 1 corresponds to bright (almost saturated) pixels, located at the center of the flame. Image pixels rarely belong to mask 12, usually only when a few outliers are present. The key advantage of this method is that it is simple to relate the features to the original image, helping the interpretation of results.
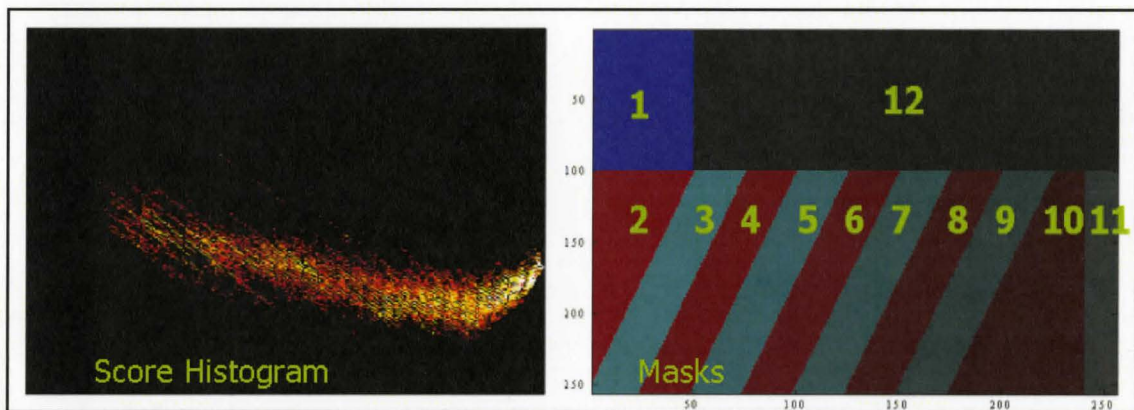
Figure 3.8: A typical score histogram and the 12 Masks applied to score histogram image

The masks only isolate a region of the score histogram. It is possible for the entire histogram to shift up or down the column length, while falling into the same masks. To capture this information, the median pixel location in each column was calculated. The range of each score histogram column that contain image pixels is also calculated. This is illustrated in Figure 3.10. Although there are 256 columns in a score histogram, the median location and range was only calculated for columns 25, 50, 75, 100, 125, 150, 175, 200, 225, and 250 since the values from column to column are highly correlated. Including the range and median location information adds 20 features to the 12 mask features. These 32 features are then
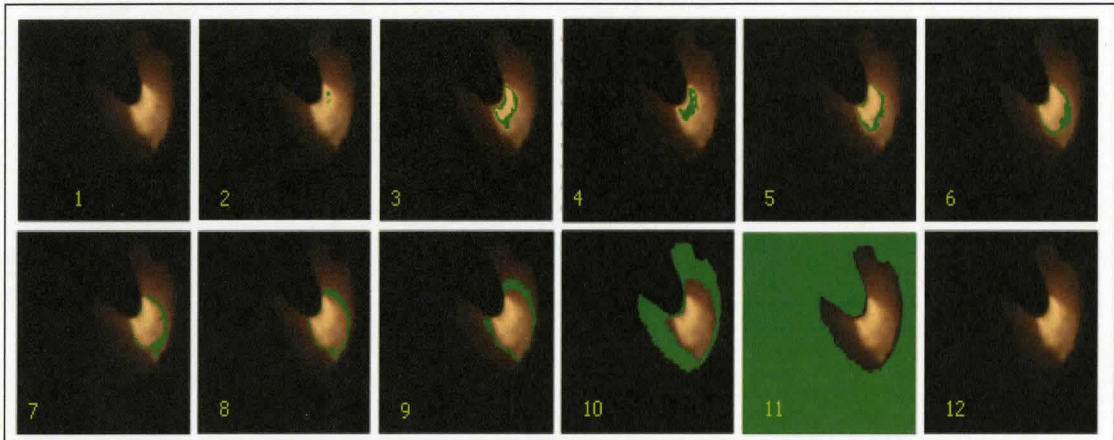
Figure 3.9: Pixels of a kiln image corresponding to masks

correlated to firing end temperature in a PLS model.

Results of PLS models

Separate PLS models were built to predict the firing end temperature using five minute averages of the features calculated in the three methods described previously. The features were used to predict FET at the current time, 1 hour and 2 hours into the future. These models were built using a training set and two validation sets. In order to determine the optimal number of PLS model components, the sum of the squared prediction error divided by the number of observations in each dataset is calculated after a model is built. The number of components that minimizes the error on all three datasets is selected. This method ensures that over-fitting of the training data is avoided.

The training and validation data used consisted of five minute averages of the image features. These were used in the models to increase the signal to noise ratio as noise from image to image is introduced when the kiln rotates. Figure 3.11 presents the average RGB values of one day of images taken every 10 seconds as well as the 5 minute average values. It is clear from this figure that filtering the data using 5 minutes creates a smoother signal.
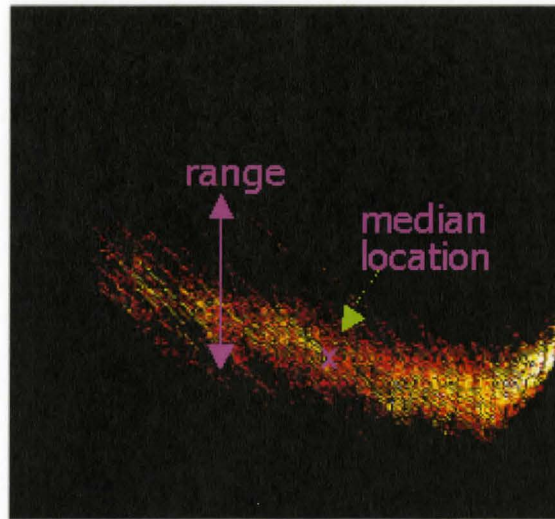
Figure 3.10: Illustration of column range and location feature calculation

The PLS model results are shown in Table 3.2. The mask method provides the best prediction, independent of the time horizon. This means that the features extracted in this method are most relevant to temperature prediction. Figure 3.12 presents these time-series plots for each data set of the mask method. These plots show that the models can predict steady-state values well, but prediction of transitions in the process are poor, especially when predicting 2 hours in advance. These models do not include any dynamic data which may explain the poor prediction during process transitions.

Incorporation of Dynamic data

The goal of including dynamic information in the PLS models is to improve prediction during process transitions, especially for prediction 2 hours into the future. These models were built using the mask image features and past values of FET and dynamics were incorporated as shown in Equation 3.2 The prediction error results of the 2 hour models with and without dynamic information are presented in Table 3.3. The prediction does not improve. Model coefficients B and C from equation 3.2 were zero, meaning that image information from more than 2 hours in the past does not provide any information for FET prediction.
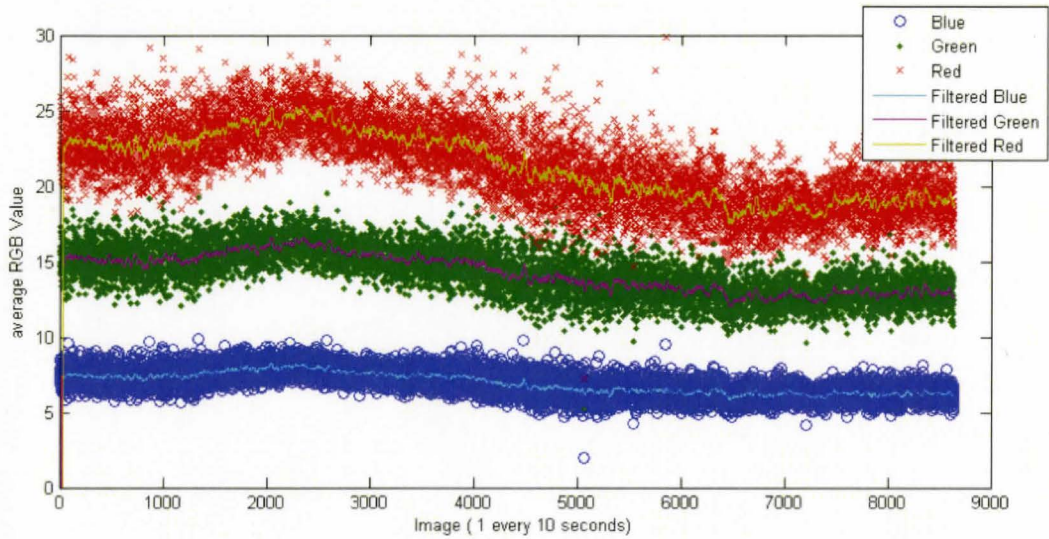
Figure 3.11: Average RGB values for 1 day of data and 5-minute filtered values

$$FET_t = A*Mask_{(t-z)} + B*Mask_{t-z-1h} + C*Mask_{t-z-2h} + D*FET_{(t-z)} + E*FET_{t-z-1h} + F*FET_{t-z-2h}$$

(3.2)

where

- A-F are model parameters calculated by PLS

- z is the number of hours into the future the model predicts (either 0, 1 or 2)

- t is time

To understand the information contained in the images further, a model was built to predict FET using mask image features every 20 minutes starting at t-20 minutes to t-4 hours. The PLS coefficients for Mask 8 are shown in Figure 3.13. It is clear that images greater than 2 hours and 20 minutes no longer provide information for FET prediction. Thus, images alone cannot be used to provide an accurate prediction 2 hours into the future. In Section 3.3.4 process data and mask images will be combined to predict FET 1 and 2 hours into the future. Dynamics are also incorporated in the models in that section by using first

Table 3.2: Feature Model Results: Sum of squared prediction error / N *100

Model	Training Set	Testing Set 1	Testing Set 2	Average
t + 0 hours: RGB	0.30	1.51	2.11	**1.31**
t + 0 hours: Hist	0.13	0.25	0.70	**0.36**
t + 0 hours: Mask	0.08	0.54	0.21	**0.27**
t + 1 hour: RGB	0.32	1.13	2.04	**1.16**
t + 1 hour: Hist	0.20	0.15	0.91	**0.42**
t + 1 hour: Mask	0.18	0.08	0.69	**0.23**
t + 2 hours: RGB	0.50	0.42	2.44	**1.10**
t + 2 hours: Hist	0.25	0.16	1.49	**0.65**
t + 2 hours: Mask	0.13	0.31	1.45	**0.63**

order plus deadtime models of both process and image data. Using the method described in Section 3.3.2, the average time constant and deadtime of the mask image features were calculated from the model shown in Figure 3.13. The deadtime is 0 minutes and the time constant is 45 minutes.

Table 3.3: Dynamic Model Results 2 hours into the future: SSPE / N *100

Model	Training Set	Testing Set 1	Testing Set 2	Average
Mask Method	0.13	0.31	1.45	**0.63**
Mask Method and Dynamics	0.13	0.33	1.47	**0.65**
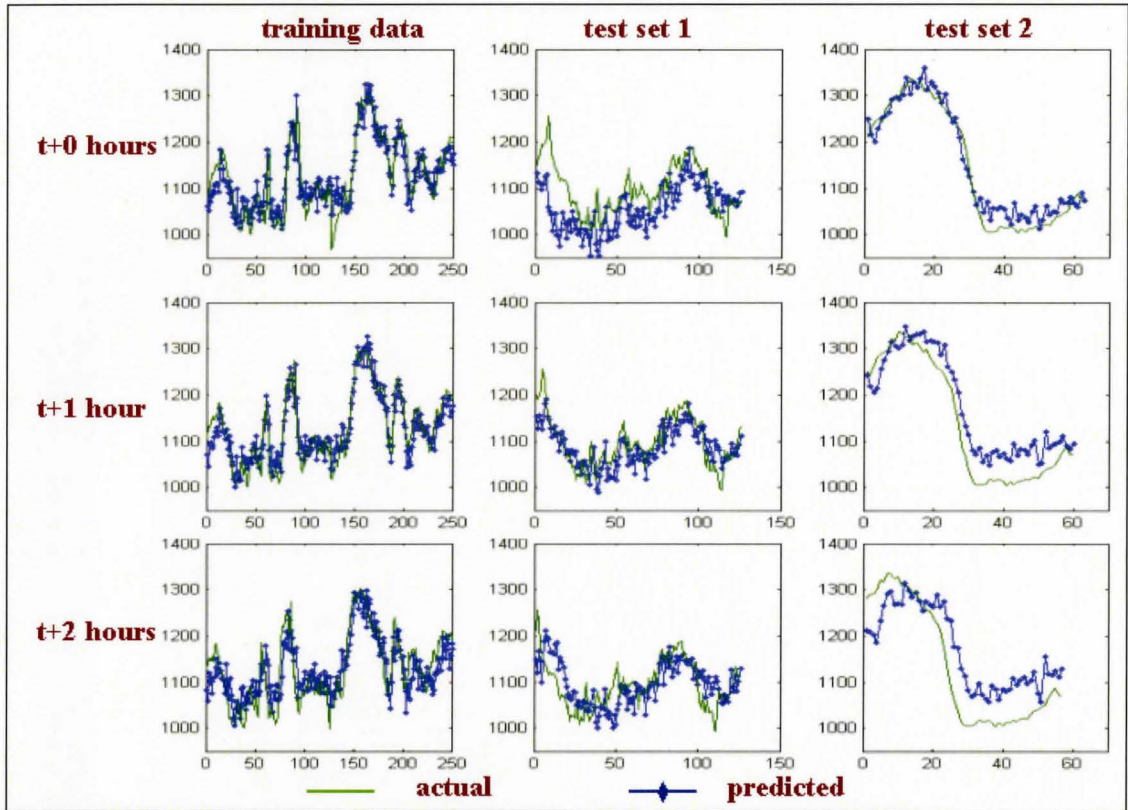
Figure 3.12: Actual and predicted plots of FET models for mask method
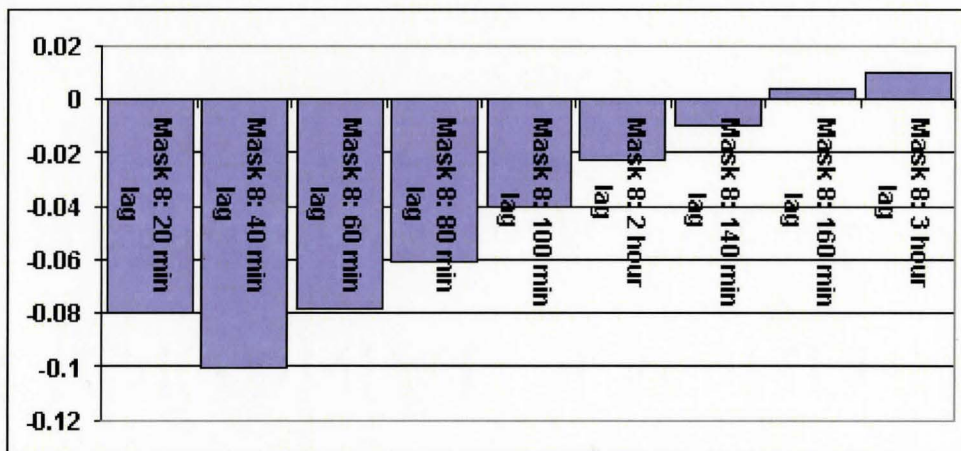
Figure 3.13: PLS Regression Coefficients of Mask 8 for FET prediction

3.3.4 Firing End Temperature prediction using mask method image features and process data

The previous section (3.3.3) showed that the mask method provided the best fit for FET prediction using images. The mask method features will now be combined with process data to provide a model that predicts FET 1 and 2 hours in advance.

The process data that are available for this model were presented in Section 3.2.2. Many of these measurements frequently spike (due to instrument plugging), contain drift and are generally noisy. Preliminary models were built after outliers were removed from the data set. However, performance was poor on test-sets due to drift in the variables. Using these variables in an online model would require advanced filtering to remove spikes and account for drift. To avoid the need for online filtering, only the manipulated variables (mud, air and oil flow) are used as process measurements. These variables contain little noise and would only require minimal supervision in an online system.

In order to provide an accurate prediction of FET some time into the future, the model must account for the long process dynamic seen in the kiln. The first-order dead time and time-constant model parameters identified in Section 3.3.2 for the manipulated variables and Section 3.3.3 for the image features are applied to each variable to create a dynamically reconciled value for the variable. Equation 3.3 presents the performed calculation and Figure 3.14 presents the first-order plus dead time model being applied to a change in oil flow. These new parameters (one for each manipulated variable and each image feature) are used to create a PLS model for FET prediction. During model building it is assumed that no change in manipulated variables are made between the current time and prediction horizon (1 or 2 hours).

$$P_{dr,t} = exp(-T/\tau_{MV}) * P_{dr,t-1} + (1 - exp(-T/\tau_{MV}) * P_{t-1-\Theta_{MV}} \tag{3.3}$$

where:

- MV is the manipulated variable or image feature

- P_{dr} is the new dynamically reconciled parameter calculated for each MV or image feature

- Θ is the dead-time

- τ is the time constant

- T is the time step
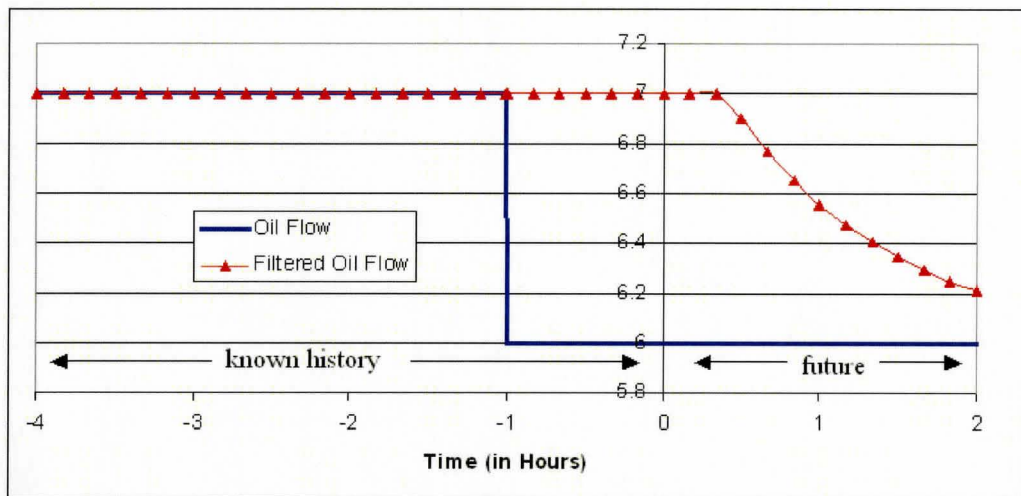
Figure 3.14: Illustration of variable filtering

To build the model that combines manipulated variable information and mask image features, a training dataset was used for model building and two test sets were used for validation. The datasets are all composed of time series data sampled at 20 minute intervals and are identical to the datasets used for the image feature models in Section 3.3.3. During model building, the number of PLS components are again selected such that the sum of squared prediction error is minimized for all three datasets. The following PLS models are built and compared to image only models (with no dynamic reconciliation):

- t+1 hour: Dynamically reconciled image features

- t+1 hour: Dynamically reconciled image features and process data

- t+2 hours: Dynamically reconciled image features and process data

The results of the PLS models are presented in observed vs predicted plots (Figures 3.15 and 3.16) and sum of squared prediction error tables (Table 3.4 and 3.5). The one hour models are very successful, tracking transitions very well. The inclusion of the process data provided little prediction improvement in these models. However, process data provides significant improvement for the two hour models. Some delay in capturing the dynamics is still present in this model. Despite this, the industrial sponsor, Irving Pulp and Paper, was pleased by the results of these models and will proceed with online implementation of both the one hour and two hour dynamically reconciled process and image data models (discussed in Section 3.4). The performance of both models will be studied to determine how best to use this new information.

Table 3.4: Combined Model Results, t+1 hour: SSPE / N *100

Model	Training Set	Test Set 1	Test Set 2	Average
Images Only	0.061	0.179	0.690	**0.310**
Filtered Images	0.057	0.212	0.495	**0.254**
Filtered Images and Process Data	0.055	0.20	0.479	**0.244**

Table 3.5: Combined Model Results, t+2 hours: SSPE / N *100

Model	Training Set	Test Set 1	Test Set 2	Average
Images Only	0.13	0.31	1.45	**0.63**
Filtered Images and Process Data	0.088	0.319	0.692	**0.366**
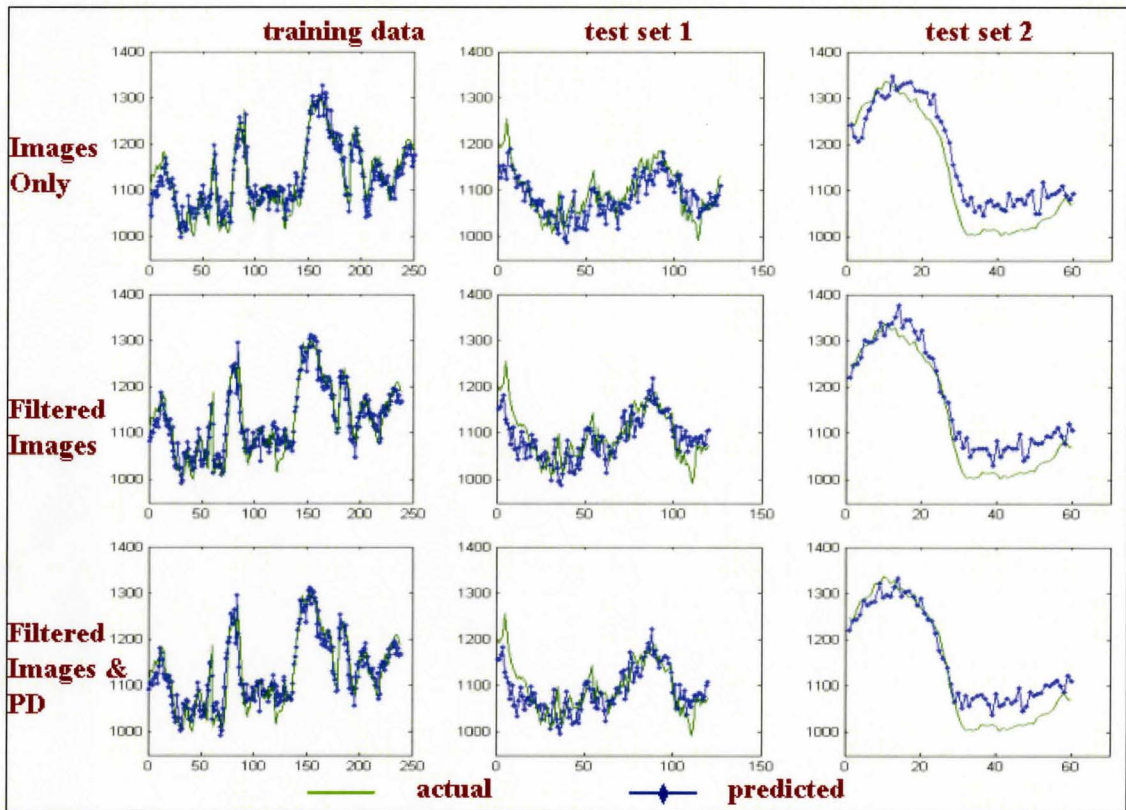
Figure 3.15: Actual and predicted plots for 2 hour FET models with and without images
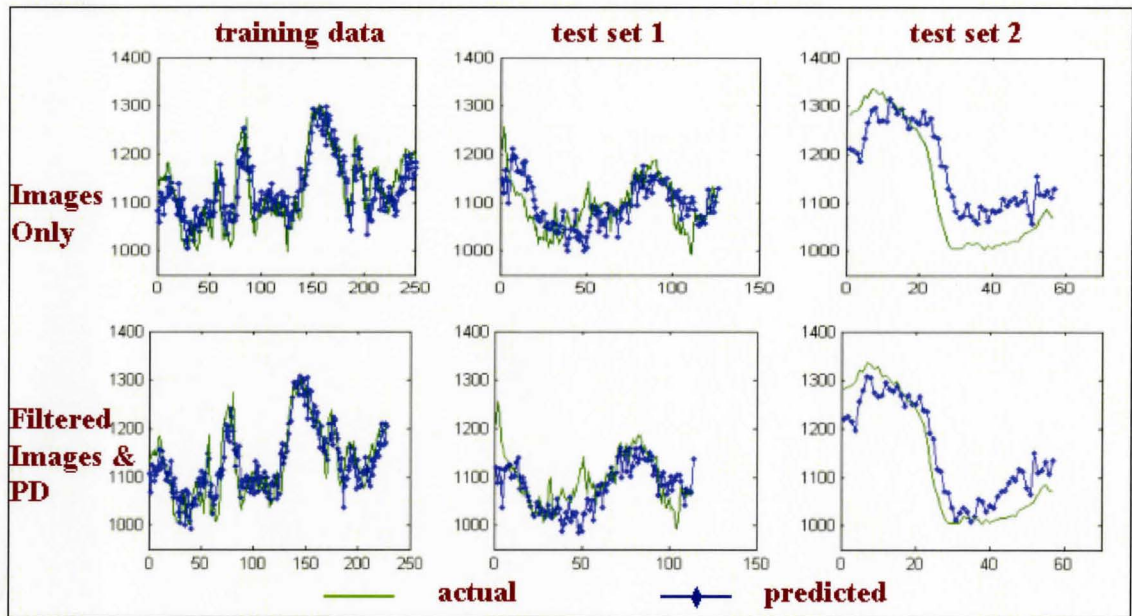
Figure 3.16: Actual and predicted plots for 2 hour FET models with and without images

3.3.5   Flame Stability Analysis

Sections 3.3.4 and 3.3.3 show that camera images can be used successfully for firing end temperature prediction. The images also contain additional information that can be used to improve lime kiln operation. The length and stability of the kiln flame is of critical importance for prevention of ring formation along kiln walls. Ring formation results in decreased productivity and expensive plant-wide shutdowns for maintenance. As alternative and cheaper fuel source are considered for use, a method to monitor and control flame length and stability is essential to reduce capacity losses and stabilize kiln operation.

At this point, any inference of flame length from the kiln images cannot be verified with physical or theoretical measure of flame length is available. Collaboration with the University of Toronto to relate image flame length to a theoretical flame length will be completed beyond the scope of this thesis. There is strong evidence that features can be extracted from the images that relate to flame length. For example, the masks that were identified in Section 3.3.3 identify pixels in rings around the flame (refer to Figure 3.9). Figure 3.17 presents a larger view of the corresponding pixels of Masks 6 and 8 in an image. It is possible that these masks can be used to determine flame length. The ratio of the number of pixels in Mask 8 to Mask 6 (shown in Figure 3.18) may be a good indication of flame length.

This work focuses on reducing the variance in firing end temperature, which would help stabilize the flame and its length. It may be necessary to incorporate mask ratios into an online implementation if kiln ringing issues are not resolved by controlling only FET.
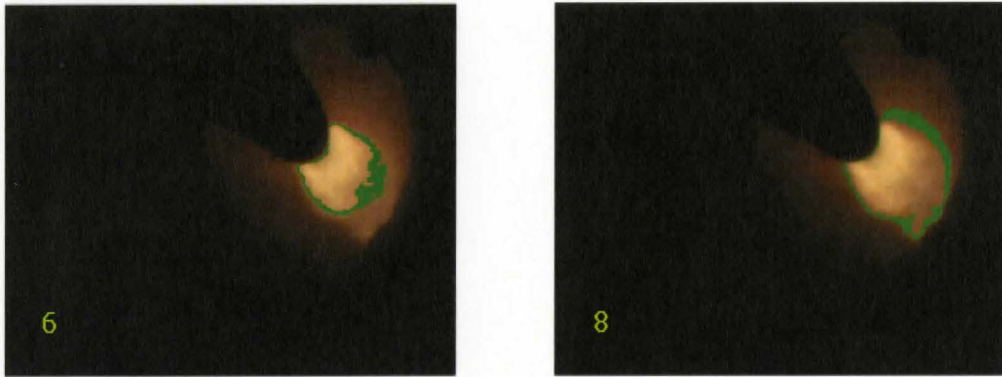
Figure 3.17: Corresponding pixels of Mask 6 and 8 in an image
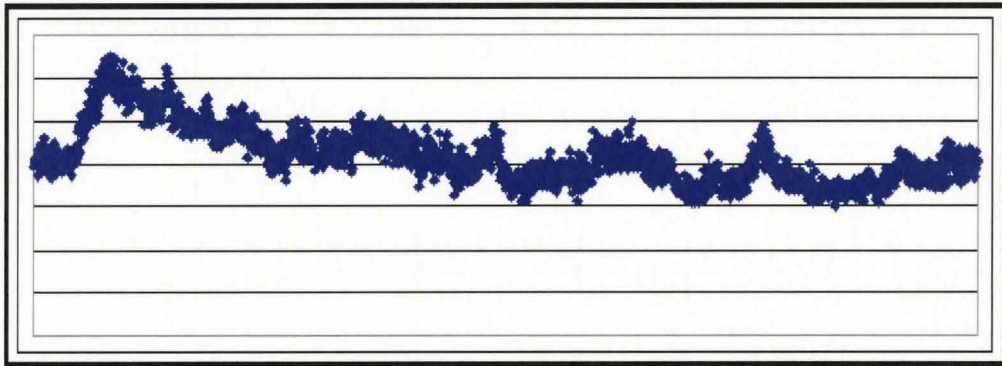
Figure 3.18: Ratio of Mask 8 pixels to Mask 6 pixels throughout the performed experiments

3.4   Online Implementation

The main goal of this study was to place the firing end prediction model developed in Section 3.3.4 online. A successful prediction of FET 1 hour or 2 hours in advance could be used in either a monitoring system or for closed-loop control. In the supervisory system, the operator would be able to see how a change in manipulated variables is expected to impact FET in 1 and 2 hours time. This could prevent the operator from making control removes that are too aggressive, which is currently a problem. A model predictive control system is also a possibility. Such a system would control the firing end temperature and exit gas temperature and composition. The firing end temperature set point would be varied based on the desired residual calcium carbonate value.

There are several challenges before online commissioning of this model, the main one being the availability of stable images over time. Online implementation was delayed by operations increasing camera brightness settings between the time that the experiments were performed and the commencement of online implementation. This required re-tuning of the model. A major process upset also occurred that resulted in dust generation inside the kiln, which completely alterers image quality. Following this, the camera failed and was replaced. It is now believed that the camera settings are stable and new models are being tuned. Once the models are placed online, the need for bias correction and / or adaptive modeling will be assessed. It is anticipated that adaptive modeling will be required as the images and process data may drift over time. Missing data will be implemented as discussed in Section 2.2.3. This remaining work will be completed outside this thesis, through the author's employer, ProSensus Inc.

3.5   Conclusions and Recommendations

In this chapter multivariate analysis of images and process data were applied to a rotary lime kiln process. Challenges of rotary kiln operation include poor process control due to long dynamics and frequent fouling (ringing) of the kiln walls. With increased energy costs

and environmental concerns, the use of alternate fuels such as biomass is of interest to these plants. Without adequate control of kiln product temperature and flame stability, the use of alternate fuels is expected to increase the existing operational challenges. The analysis of the Irving Pulp and Paper lime kiln demonstrates that multivariate image and data analysis can be used to address these issues.

Prediction of kiln product temperature (firing end temperature) and kiln product quality (residual calcium carbonate) was achieved through the use of images and process data. A four-day experiment was first performed to collect data from the process by varying production levels, air and fuel flows. With this data, residual calcium carbonate and firing end temperature were predicted and an analysis of flame stability was performed.

Residual calcium carbonate can be predicted using a simple linear relationship between it and firing end temperature. This important quality measurement is noisy and thus a more sophisticated analysis is not expected to improve predictability significantly. Instead, the focus was on predicting FET in advance, which can then be used to provide an accurate prediction of residual calcium carbonate.

Firing end temperature was successfully predicted 1 and 2 hours in advance by a multivariate analysis of both images and process data. Several approaches for extracting characteristics (features) of the images were first studied. Of the three methods studied: average RGB method, cumulative histogram method, and the mask method, it was found that the mask technique identified the best image characteristics for FET prediction. Additionally, it is simple to relate model results back to the original kiln images when using this method. This is helpful for model interpretation, both for operators and engineers. Dynamic information was incorporated in combined image and process data models by use of first-order models that identified the time constant and time-delay. A model one hour into the future predicts transitions in the firing end temperature better than a 2 hour model.

Online implementation of the one and two hour firing end temperature models is desired to evaluate performance. This was hampered by unstable camera images and will be completed outside the scope of this thesis. Once an online model successfully predicts FET, a closed

loop control or operator advisory system can be implemented to improve process control.

Many of the features identified with the mask method could also be used to monitor and control flame length and stability. A stable flame could help reduce kiln ringing and assist in achieving successful operation while using alternate fuel sources.

Finally, it was demonstrated that multivariate image and process data analysis is a promising technology for rotary kiln processes and can lead to significant operating expense reduction.

3.6 Acknowledgments

Chapter 4

Basic Oxygen Furnace Analysis

4.1 Introduction

A basic oxygen furnace (BOF) is a unit in the steelmaking process where molten iron and scrap metal are converted into refined steel. Oxygen is injected into a mixture of iron, scrap and fluxes to reduce carbon content (decarburization) and other impurities, and to increase product temperature. The high cost of oxygen makes this batch process expensive to operate. In order to minimize oxygen consumption, the batch should be completed as soon as the desired composition and temperature are reached. However, temperature and composition are not measured until oxygen flow is ceased. In many batches the process is ended after the desired end-point has been reached, which uses excess oxygen and longer processing time. Stopping the oxygen flow several times to measure composition and temperature is time-consuming and inefficient. An online soft sensor that predicts end-point properties would be a valuable tool for operations to determine when to end the batch. In this chapter, multivariate image and process data analysis are studied to predict final carbon content (the main controlled variable) of the batch.

4.1.1 Process Description

At the beginning of a batch (also called a heat), scrap from a storage yard and melted iron from an upstream blast furnace is loaded into the BOF vessel. Fluxes are also added to the vessel in the beginning stages of the heat. The types and amounts charged are determined by a charge model that accounts for the initial iron properties and final desired heat composition. An oxygen lance is then lowered into the vessel and the heat is begun. During the heat, there are three phases: pre-ignition, mixing controlled decarburization phase, and diffusion controlled decarburization phase. They are labeled on a plot of off-gas CO_2 concentration versus time (Figure 4.1). The end of the heat is where the carbon composition of the metal changes most drastically, as shown by the rapid decline in off-gas CO_2.
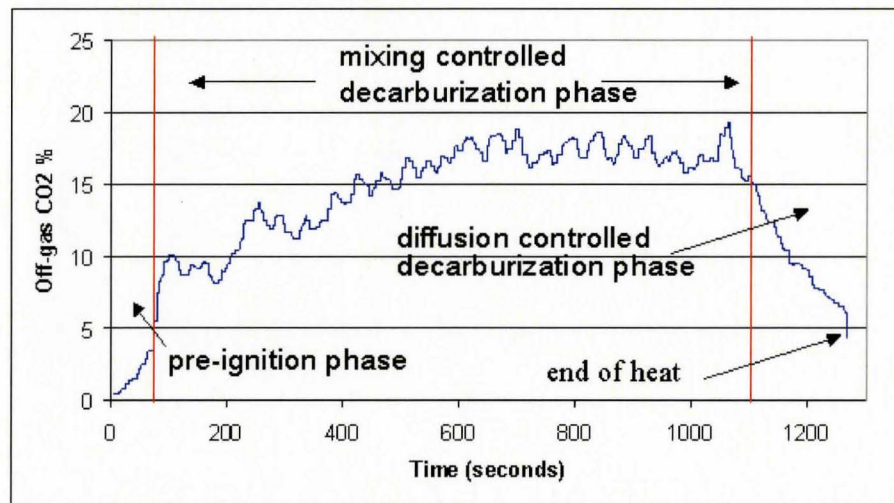
Figure 4.1: Phases of a BOF heat identified on a typical off-gas CO_2 vs time plot

Throughout a heat the height of the oxygen lance and oxygen flow are controlled by operations. Normally these parameters are set by the charge model but at times material may splash (slop) over the top of the vessel if there is too much energy in the vessel. The operator must reduce oxygen flow and increase the lance height to bring the process under control. A BOF is a unique combustion process because there is a gap between the vessel and gas collection system (refer to Figure 4.2), allowing operators to closely monitor for slop

conditions from the control room. The flame visible at the gap is also used to determine carbon in the heat. The flame gets darker towards the end of the heat, which signifies a decrease in carbon. This information along with the amount of oxygen that has been injected into the vessel and the cooling system steam flow helps the operator determine when to end the heat. Once the end-point properties have been achieved, the vessel is tipped and the contents are emptied into ladles for further processing.

The work in this chapter is being performed in collaboration with Tenova Goodfellow Inc., ProSensus Inc, and U.S. Steel Hamilton Works. Process data analysis has already been completed and preliminary models are online to predict end-point carbon and temperature. Though some success has been achieved (within the desired error for approximately 80% of the heats) the inclusion of image analysis is being studied to improve the carbon model. Prediction within 0.01% of the measured carbon content is desired.
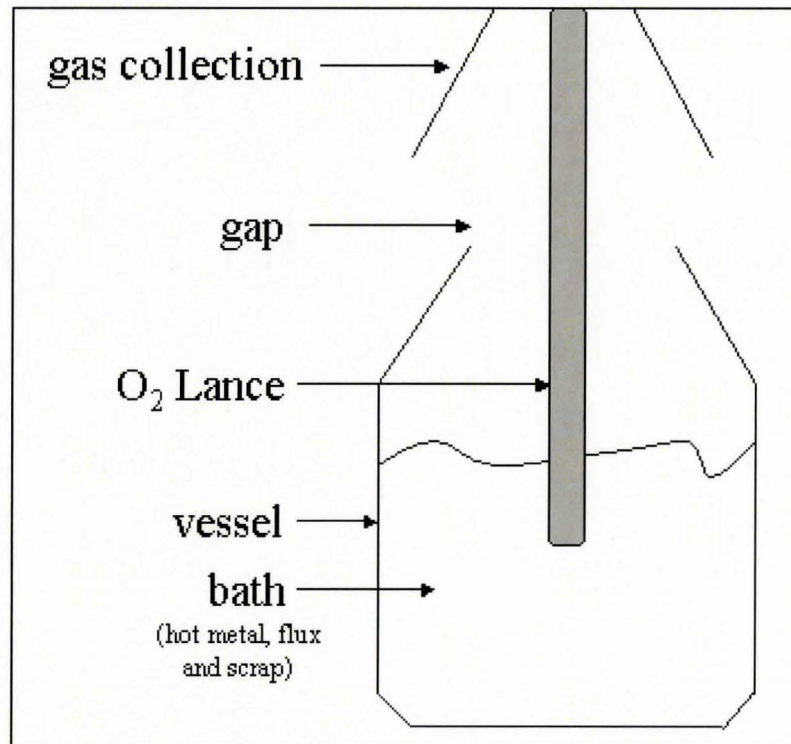
Figure 4.2: Diagram of basic oxygen furnace

4.2 Data Available

This section will provide an overview of the process and image data available. Measurement noise and instrumentation challenges are also addressed here.

4.2.1 Vision System

Cameras are not generally installed at a basic oxygen furnace because the gap flame is clearly visible from the control room. However, in order to perform this study a camera was required and therefor installed. An advantage of the gap flame being visible from a distance is that a camera does not require contact with the flame. Such a camera needs less cooling, less maintenance and is cheaper than a camera that is installed directly into a furnace wall. The camera installed for this study is a high-temperature surveillance camera manufactured by JM Canty ® [JM Canty Inc. [2008]]. This camera was selected due to its low cost, low maintenance requirements and ease of installation.

The camera provides good quality digital images as shown in Figure 4.3. However, selecting the optimal camera settings (gain and exposure time) is difficult. At the beginning and end of the heat the flame is quite dark and during the middle of the heat (mixing controlled decarburization phase) it is extremely bright. The ideal camera settings would prevent saturation in the middle of the heat while also avoiding a completely dark image at the beginning and end of the heat. Such a setting was not possible in this process. Instead, the focus was placed on obtaining ideal images during the diffusion controlled decarburization phase, as it provides the most information about carbon content.

There are further challenges that exist with the imaging set-up that will be addressed in Section 4.3.1. These are:

- Changing field of view: results from vessel not always returning to the same position and build-up on top of the vessel over the course of a heat.

- Build up on furnace ceiling over the course of the heat
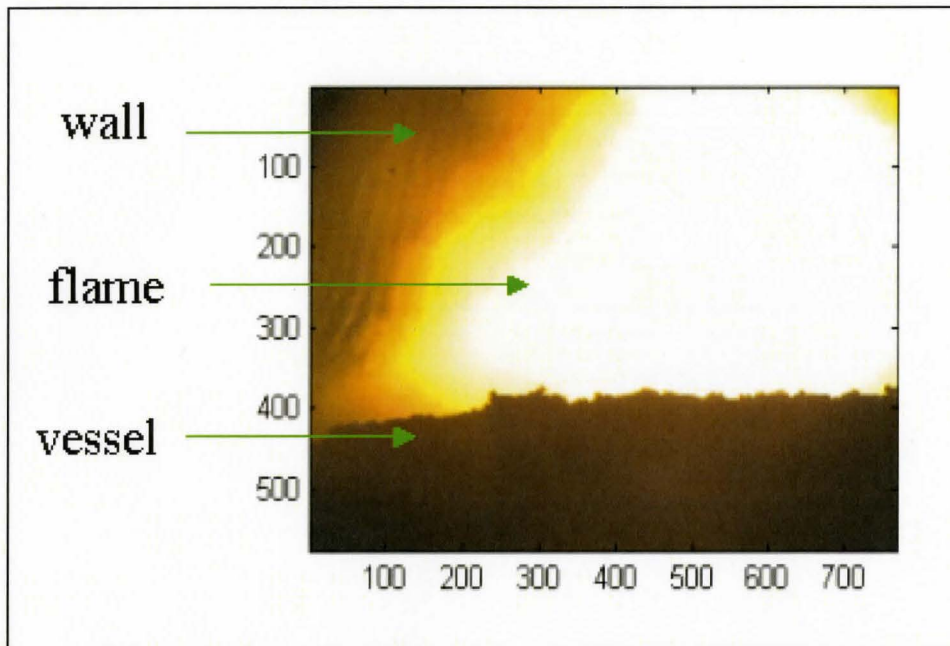
Figure 4.3: Example of image provided by the JM Canty® camera

4.2.2 Process Data

There are various process measurements available on a basic oxygen furnace. For this analysis, the measurements are divided into initial conditions (Z), trajectory variables (X), final quality variables (Y).

Initial Conditions:

- raw material amounts (scrap, hot metal, fluxes)
- hot metal chemistry and temperature
- ignition time

Trajectory Variables:

- steam flow

- oxygen flow

- off-gas chemistry

- exhaust draft

- lance height

Final Quality Variables:

- metal temperature

- metal carbon or oxygen content

The final metal chemistry and temperature are measured by dropping a 'bomb' into the bath after the oxygen lance is removed. These are manufactured by Heraeus Electro-Nite (Heraeus Electro Nite [2009]). Signals from this sensor for temperature and oxygen content are sent to the control system before the it is consumed by the bath. The carbon content of the bath is calculated from the oxygen content using the non-linear relationship presented in Figure 4.4. This method of measuring the final quality is relatively new at this plant. Previously, the vessel was tipped and temperature was measured and a sample of the metal was sent to a lab for chemical analysis. The same Heraeus sensor is used, but instead of being dropped into the bath it is attached to a long sampling pole. This method is being phased out as it was time consuming. Though the bomb measurement is much quicker, it contains high error due to bath mixing and improper penetration of the slag layer. To quantify this error, three repeats were performed for three different heats shortly after the lance was pulled. The results are shown in Tables 4.1 to 4.4. The standard deviation of the carbon measurement is 0.0034%, which is high. The 95% confidence interval on this measurement is +/- 0.0068%. The goal of this project is to predict carbon within 0.01%, and the measurement error takes up 68% of this range. These large errors clearly make accurate prediction difficult, though every effort is being made by operations to improve this measurement.

Table 4.1: Repeat bomb measurements for heat 1

Bomb	Time	ppm O2	Carbon	Temp
1	0s	687.1	0.046	2977
2	+30s	687.8	0.046	2949
3	+1m25s	581.7	0.052	2963
Standard deviation		**61.1**	**0.003**	**14.2**
Range		**106.1**	**0.006**	**28.3**

Table 4.2: Repeat bomb measurements for heat 2

Bomb	Time	ppm O2	Carbon	Temp
1	0s	923.7	0.037	3060
2	+1m	1166	0.031	3082
3	+2m	1020	0.034	3069
Standard deviation		**122**	**0.003**	**10.6**
Range		**242.3**	**0.006**	**21.0**

Table 4.3: Repeat bomb measurements for heat 3

Bomb	Time	ppm O2	Carbon	Temp
1	0s	888.7	0.038	3015
2	+45s	713.8	0.044	3010
3	+1ms			3018
4	+1m30s	892.5	0.038	2998
Standard deviation		**102.6**	**0.004**	**8.7**
Range		**179.5**	**0.007**	**19.7**
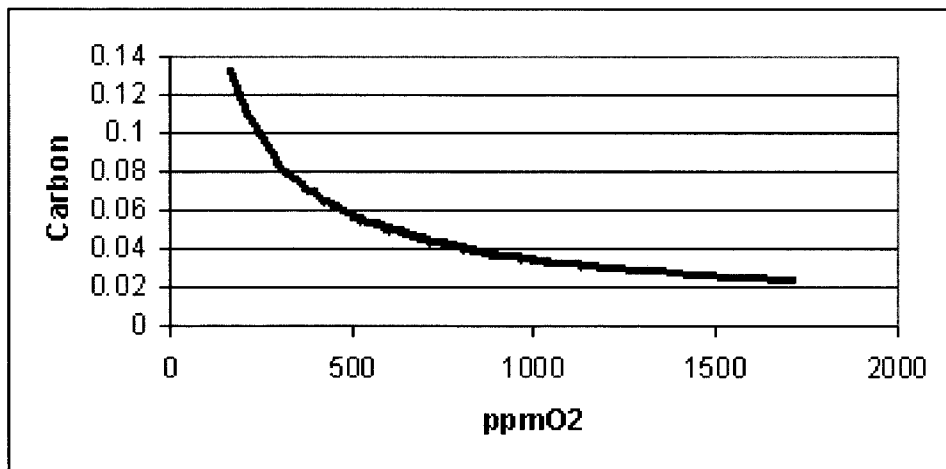
Figure 4.4: Carbon and ppmO2 relationship

Table 4.4: Average range and standard deviation of the bombs

Parameter	ppm O2	Carbon	Temp
Average Range	176	0.0062	23
Average Standard Deviation	95.2	0.0034	11

4.3 Results and Discussion

Image and process data for a total of 50 heats were collected during two time periods. This section presents the various steps that were required to create a successful carbon prediction model. Image pre-processing, image feature extraction, image only PLS models for carbon prediction and combined process data and image feature models are discussed.

4.3.1 Image Pre-processing

As mentioned in Section 4.2.1, the camera's field of view changes throughout the heat as well as between successive heats. When the vessel is tipped to empty the contents at the end of the heat, it is not always replaced to the exact same location. Additionally, buildup can occur at the top of the vessel during a heat, either if slopping occurs or if material that has built up on the furnace ceiling deposits onto the vessel. The buildup on the top of the furnace can also obstruct the camera's view. These concerns are depicted by images of three separate heats in Figure 4.5.

To address the changing field of view, the top of the vessel was first identified with traditional image analysis. There is a large difference in colour between the flame and the vessel during the second phase, facilitating edge detection. A canny edge detector (Glasbey and Horgan [1995]), available in MATLAB ®, was successfully employed for this purpose. The edge is identified once per heat, as close to the end of the heat as possible. This ensures that the identified edge will be as accurate as possible throughout the end of the heat since buildup on the vessel can still occur then. As the images begin to darken due to significant carbon depletion, edge detection is more difficult. The edge is thus identified for the last image in

the heat where the average red colour channel value of the entire frame is greater than 150. 50 rows below and 150 rows above the edge are utilized to create a windowed image used for further analysis, as shown in Figure 4.5. A similar field of view is therefor created for all of the heats studied.
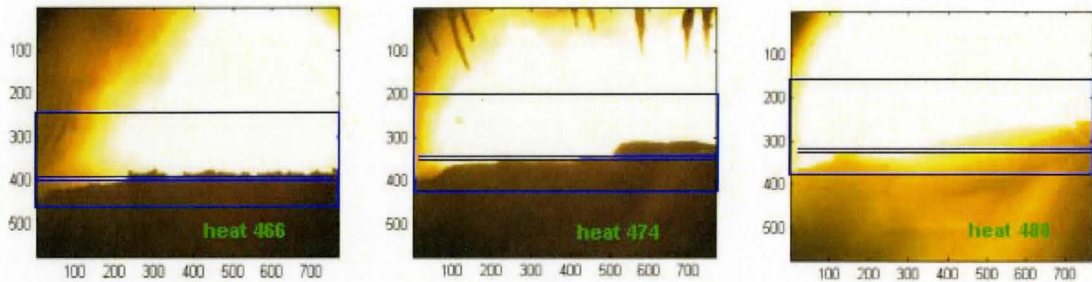
Figure 4.5: Pre-processing of images: Examples of 3 heats

4.3.2 Multivariate Image Analysis and Feature Extraction

Multivariate image analysis is performed on the windowed images by the steps described in Chapter 2. An image every 2 seconds is used for the last 120 seconds of each heat for MIA model identification. Figure 4.6 presents six images from the last two minutes of heat # 479 and Figure 4.7 presents the corresponding score histogram plots. The bright sparks in the last image are caused by the oxygen lance being removed from the bath at the end of the heat. The figures show that as the heat gets closer to completion significant darkening is observed with corresponding changes in the score plot. Extracting features from the score plots is anticipated to accurate carbon prediction since changes in the images are clearly seen in the score plots.

Image Feature Extraction

Two approaches were studied to extract features from the score histogram plots. The first method is the use of the average of the two score values, T1 and T2 of all the pixels in each image. This method is expected to be successful because the score histogram plots vary significantly as the image changes (shown in Figure 4.7). The main disadvantage of

the method is that vessel pixels are not removed from the analysis. As carbon depletion occurs, the vessel pixels also darken, which impacts the T1 and T2 plot. A second method, using score histogram masks, accounts for this change in vessel brightness.

In the mast method, 10 masks are applied to the score histograms, as presented in Figure 4.8. These 10 masks identify pixels in the image that go from the brightest (Mask 1) to the darkest (Mask 10). Figures 4.9 to 4.11 show the pixels corresponding to the 10 masks of three different images in heat 479. The first image (Figure 4.9) presents the image 120 seconds before the end of the heat, the second image is 48 seconds from the end of the heat, and the third image is 10 seconds from the end of the heat. Since the overall image darkens closer to the end of the heat, the vessel pixels always fall into a different mask. To address this, the vessel pixels need to be identified and removed from the analysis using the masks. Prior to carbon depletion, when the image is very bright, all of the pixels except for the vessel pixels belong to Mask 1. This can be observed in Figure 4.9. The average value of the red channel of all the pixels in the image is greater than 245 prior to carbon depletion. Thus, for each heat, the last image in the heat for which the average red channel is greater than 245 is first identified to be used for vessel removal. The masks are applied to the score histogram of the image, and only the pixels falling into Mask 1 are used for feature extraction for the remaining images in the heat. Since not all heats will have the same number of vessel pixels, the number of pixels falling into each mask are divided by the number of non-vessel pixels in the heat. The features can thus take on values between 0 and 1.

In addition to the mask method and T1 and T2 method, the average value of the red, green and blue channels of vessel pixels are also identified. The pixels located in rows 500 to 576 and columns 500 to 768 always belong to the furnace vessel for all of the heats. The average red, green and blue value is calculated for this region and will be incorporated into some of the PLS models.
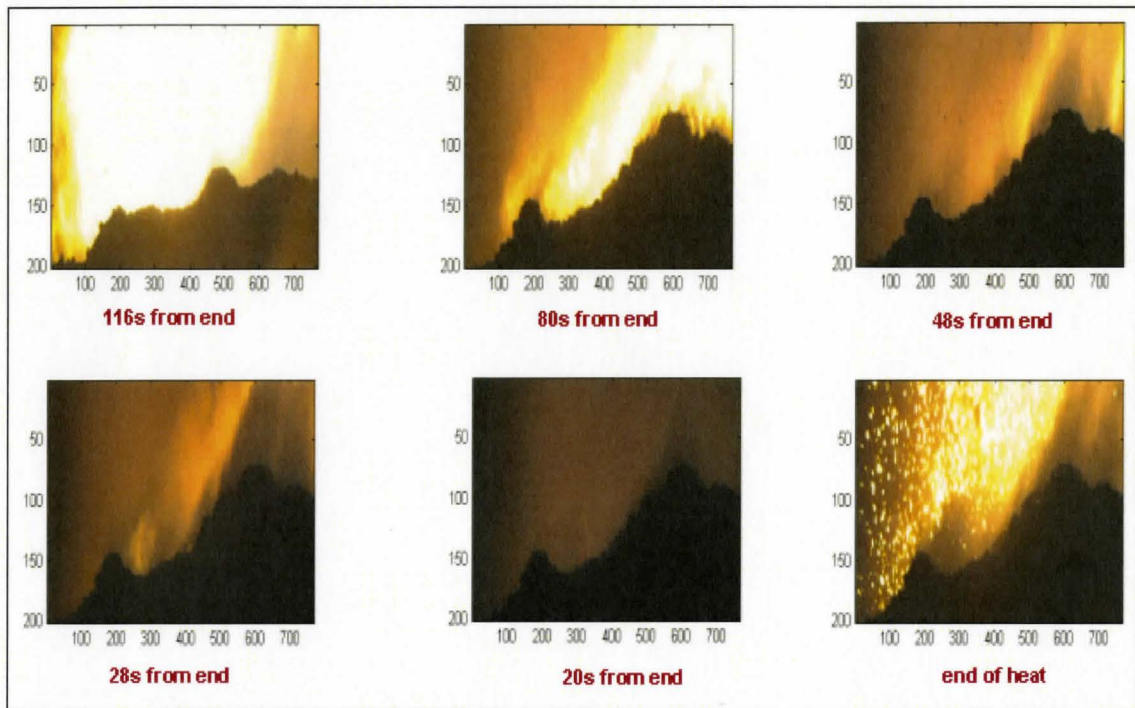
Figure 4.6: Successive images of heat 479
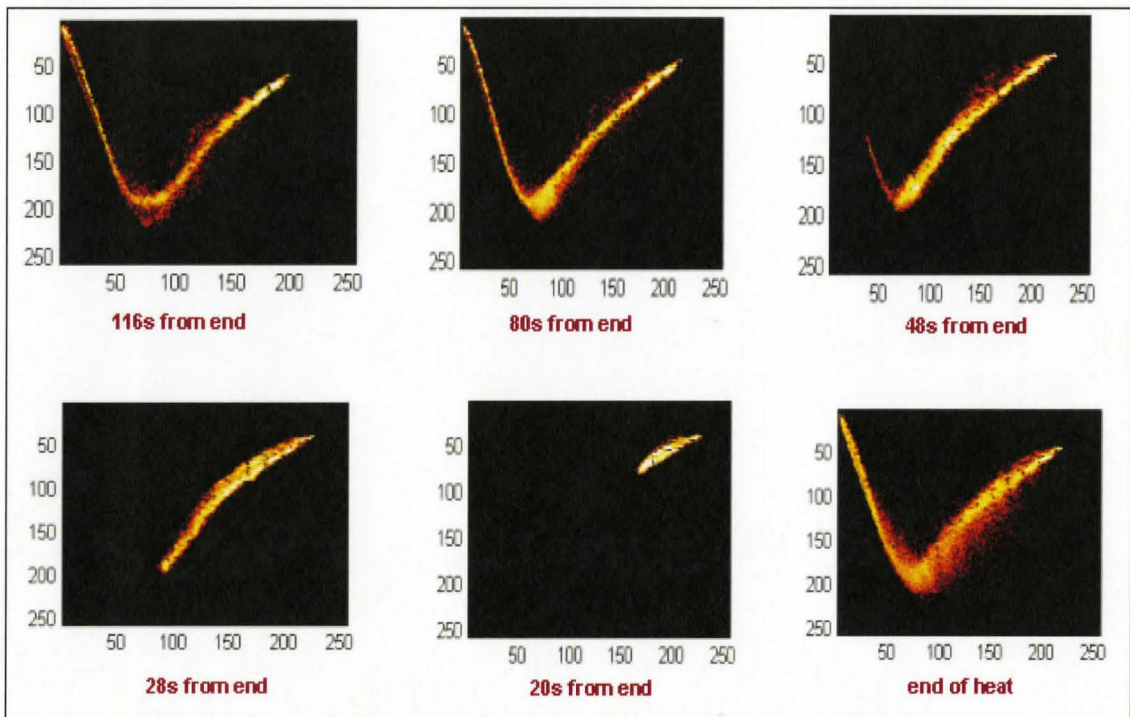
Figure 4.7: Corresponding T1T2 score images of heat 479
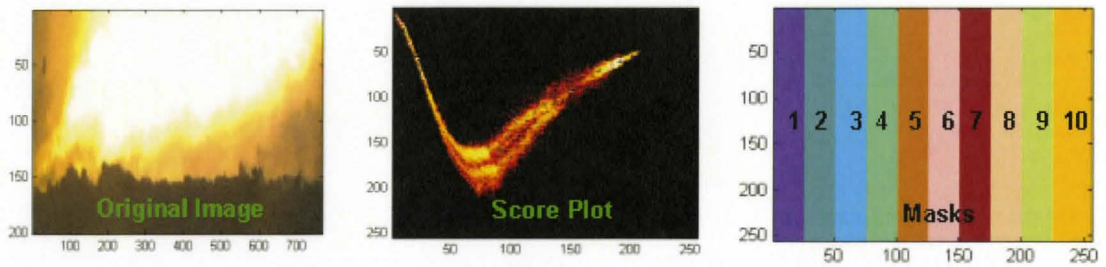
Figure 4.8: A typical image, corresponding score histogram and the 10 Masks applied to score histogram image
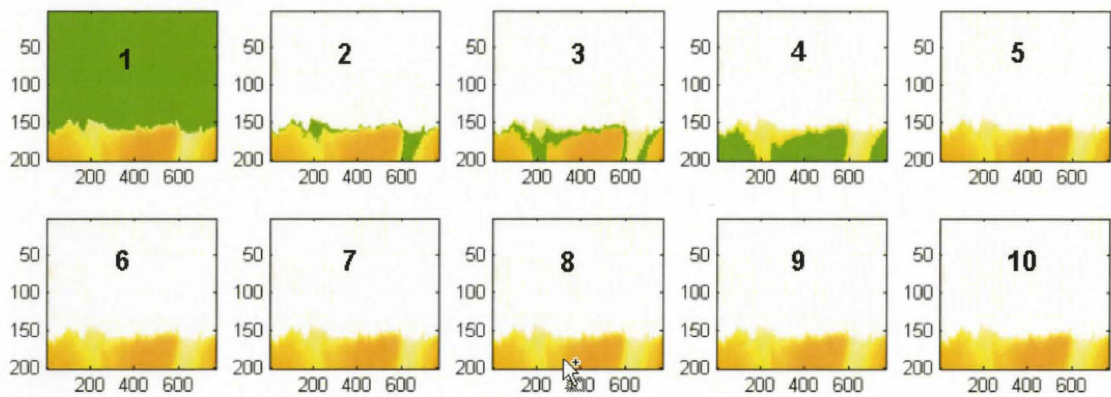
Figure 4.9: Pixels corresponding to each mask (in green) 120s prior to the end of heat 479
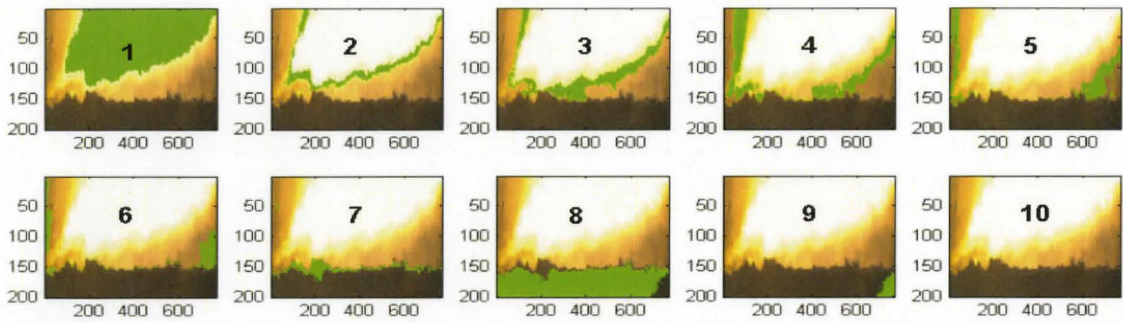
Figure 4.10: Pixels corresponding to each mask (in green) 48s prior to the end of heat 479
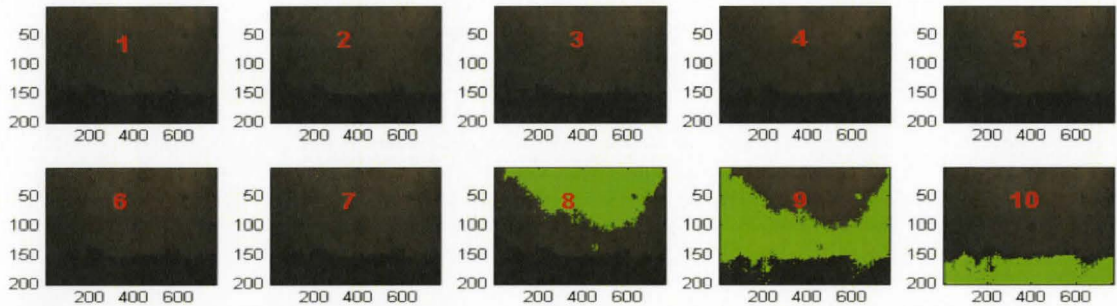
Figure 4.11: Pixels corresponding to each mask (in green) 10s prior to the end of heat 479
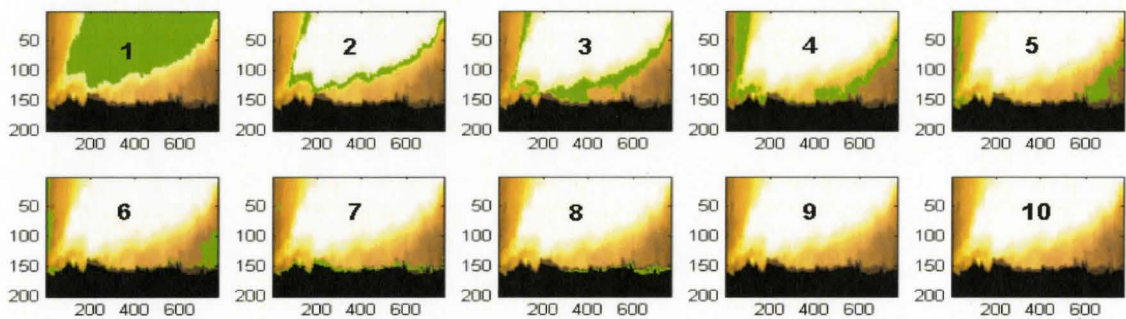
Figure 4.12: Pixels corresponding to each mask (in green) 48s prior to the end of heat 479 with identified vessel pixels in black

4.3.3 Results of Image Feature Models

Several PLS models are built to predict the end-point carbon using the features extracted from the score histogram plots. However, since this is a batch process, the feature data must first be aligned for all of the batches. None of the heats are of the same duration or have the same amount of oxygen injected over the course of the heat. As a result, the extracted image features were aligned against the last 200 units of cumulative oxygen in each heat. This is approximately 2 minutes of data, depending on the O_2 flow rate. Figure 4.13 presents the aligned average T1 feature over the last 150 units of cumulative O_2 and Figure 4.14 presents the aligned Mask 1 image feature over the same range of cumulative O_2.
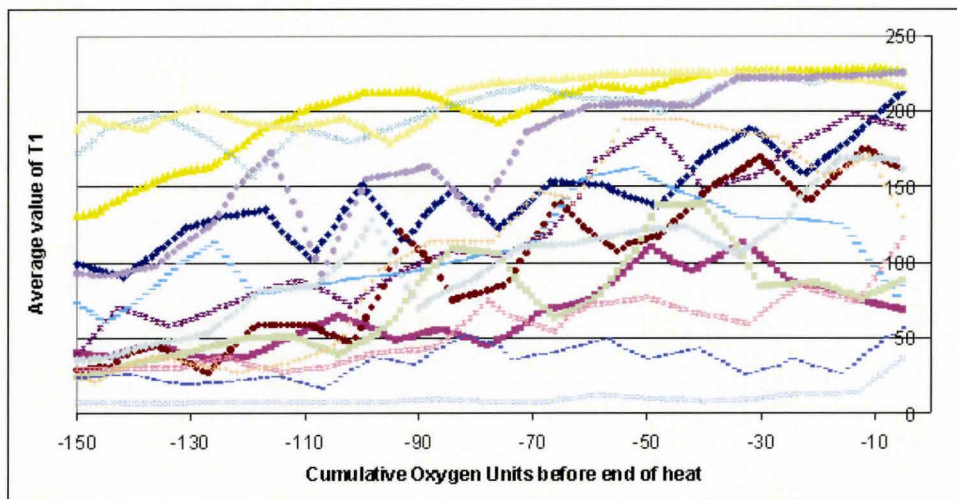
Figure 4.13: Average image T1 aligned against the last 150 values of cumulative O_2 for several heats

The extracted features are then used to build PLS models that predict carbon content. A total of 47 heats are available, with 34 being used for model training and 13 for model validation.

Two methods are used to build the models; a traditional batch or a data characteristic method. In the traditional batch approach, all of the aligned features must be decomposed
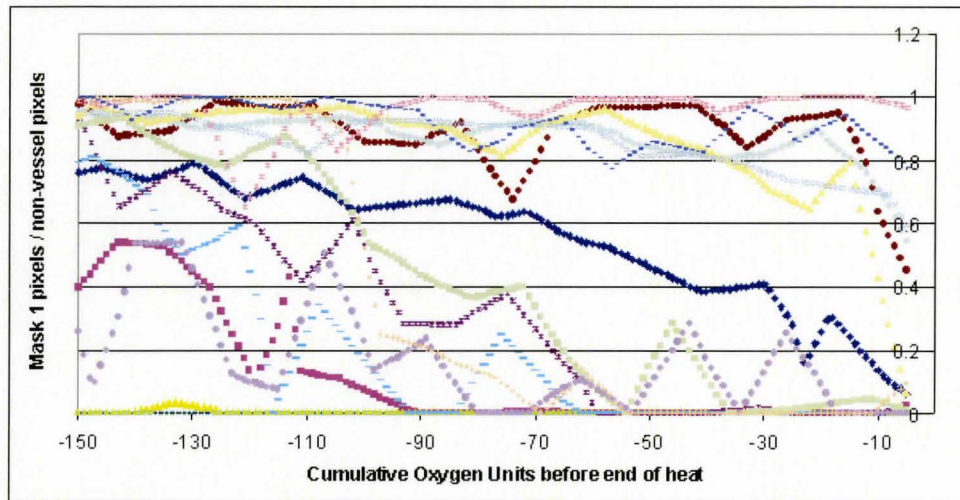
Figure 4.14: Mask 1 image feature aligned against the last 150 values of cumulative O_2 for several heats

as shown in Figure 4.15. Further details can be found in Section 2.4. For the second approach, the characteristic method, features from the aligned data are extracted instead of using all of the data. The features can include averages over a range of cumulative O_2 values, slopes, etc.. Both traditional batch methods and average values and slope characteristics are studied in this work. The PLS models that are built are:

- Model 1: Averages of the average T1 and T2 image features

- Model 2: Averages of the average T1 and T2 and slopes of average T1 and T2

- Model 3: Averages of the average T1 and T2, slopes of average T1 and T2, and average vessel RGB

- Model 4: Batch method using average T1 and T2 features

- Model 5: Average mask feature values

- Model 6: Batch method using mask feature values

For each model, the characteristics were calculated over various cumulative O_2 value ranges

as shown in Table 4.5. The characteristics were then used to build a PLS model on the training data. The model's performance on the validation dataset is evaluated by the sum of the squared prediction error (SSPE) over all of the heats. For all of the models built, the best prediction was found to be on models built between 150 and 5 units of cumulative O_2 from the end of the heat. For each data range, the number of PLS components was varied to determine the optimal amount of components to use. Table 4.5 presents the prediction error on several cumulative oxygen ranges and PLS components for Model 4 (batch method using average T1 and T2 features).
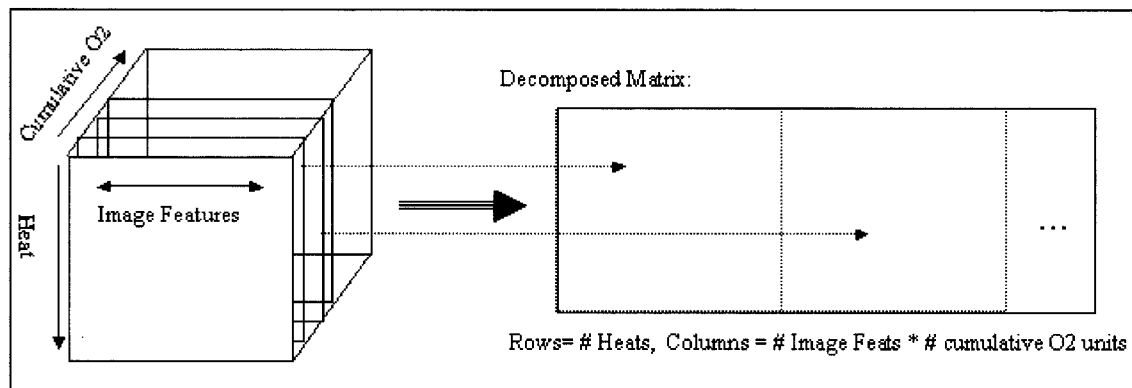
Figure 4.15: Image Feature data decomposition for batch PLS model building

The results of the 6 PLS models are evaluated in three different ways: by the sum of squared prediction error on the validation data set, the number of heats that were not predicted within the desired range of +/- 0.01%, and the observed versus predicted plots. These results are shown in Table 4.6 and Figure 4.16. Using average T1 and T2 values performs better than the mask method, which is a result of the high carbon measurement error. The mask method characterizes more features of the flame, but since the carbon measurement is erratic, it does not aid the prediction. It is likely for the same reason that a data characteristic method performs better than a batch method. Overall, Model 2, the average of the average T1 and T2 and slope method performs the best.

Examination of the predicted versus measured plots (Figure 4.16) reveals that the two heats with high values of carbon (0.07%) are not predicted well in either the training or

Table 4.5: SSPE*1000 of validation dataset for the batch T1T2 method on different cumulative oxygen ranges

Start CumO2	End CumO2	1 Comp.	2 Comp.	3 Comp.
-50	-5	0.966	0.987	1.17
-50	-40	1.095	1.132	1.437
-100	-5	0.987	1.017	1.486
-100	-40	1.030	1.058	1.896
-100	-75	1.154	1.166	1.494
-150	-5	0.910	**0.908**	1.103
-150	-40	0.934	0.927	1.121
-150	-75	0.991	0.982	1.267
-150	-110	1.008	0.987	1.013
-150	-145	1.051	1.033	0.989
-200	-5	0.946	0.912	0.986
-200	-40	0.979	0.932	1.002
-200	-75	1.037	0.988	1.053
-200	-110	1.065	1.003	0.993
-200	-145	1.117	1.062	1.062

Table 4.6: Parameters for evaluating Image models

Model	No. PLS Comp.	Valid SSPE	Valid >0.01	Training >0.01	Total >0.01
Model 1	1	0.918	1/13	3/34	4/47
Model 2	**1**	**0.873**	**1/13**	**3/34**	**4/47**
Model 3	4	0.955	2/13	3/34	5/47
Model 4	2	0.908	1/13	3/34	4/47
Model 5	1	1.029	2/13	2/34	4/47
Model 6	1	0.966	2/13	3/34	5/47

validation dataset. The models may be improved by use of a non-linear transformation on the carbon measurement. The data from Model 2 were used to build several PLS models using different transformations on the carbon measurement (shown in Table 4.7). The models were built on the combined training and validation datasets to increase the amount of data available. The measure of the prediction error used is the square root of the average prediction error (RMSE). The results are presented in Table 4.7. Unfortunatley, the largest improvement seen with a 1/y transformation is only 1.17%. This is not a statistically significant improvement. The predicted versus measured plot is shown in Figure 4.17. It could be that these two heats are outliers, however, more data is required at higher carbon levels to make definite conclusions. Model 2 will be combined with process data to build the overall model.

Table 4.7: Transformations on Carbon Measurement (y)

Transformation	RMSE	Improvement in RMSEE
None	0.007004	N/A
$\log(y)$	0.006932	1.03%
$1/y^2$	0.006927	1.11%
$1/y$	0.006922	1.17%
$1/y^{0.5}$	0.006923	1.17%
$1/y^{0.25}$	0.006926	1.12%
$y^{0.25}$	0.006942	0.89%
$y^{0.5}$	0.006957	0.68%
y^2	0.007212	-2.96%
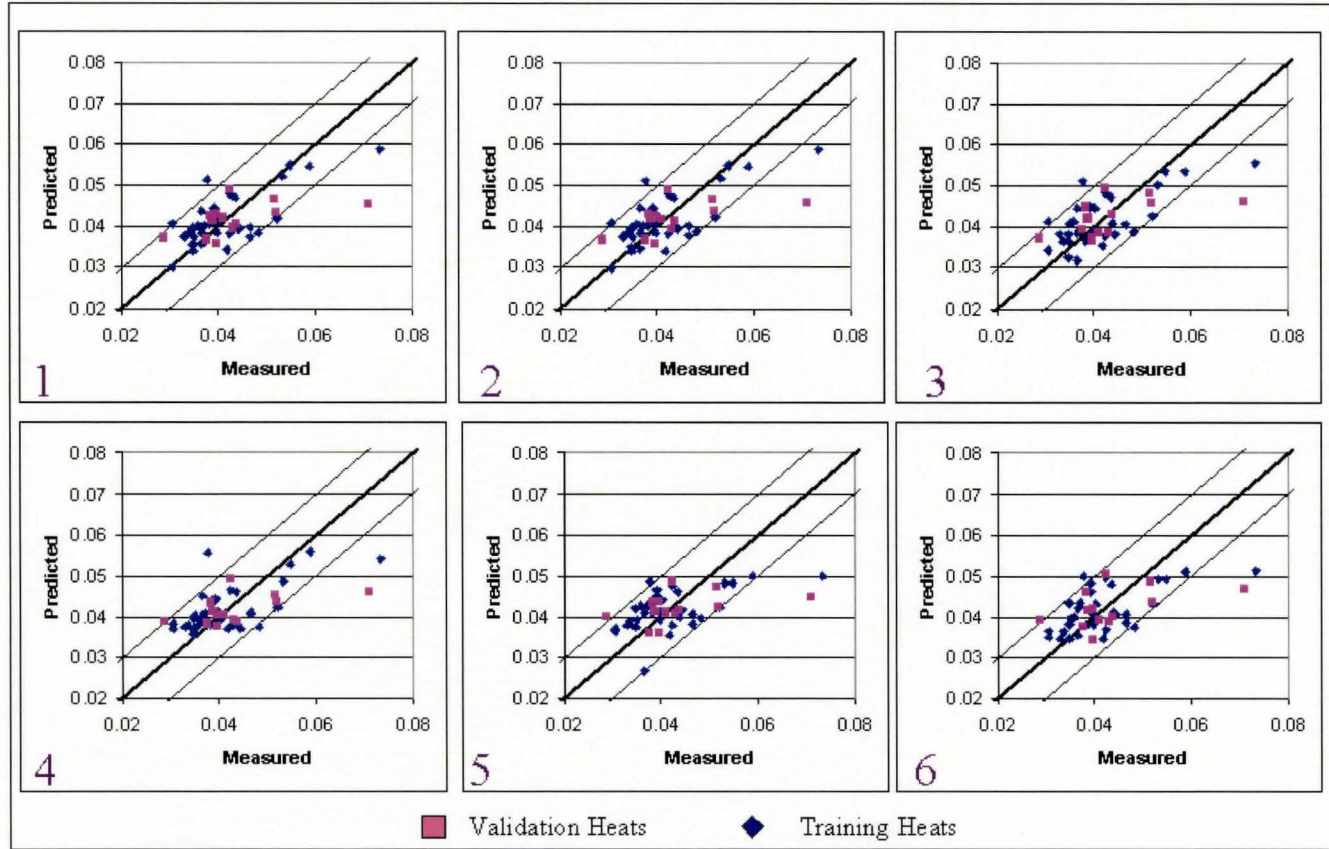
Figure 4.16: Observed vs Prediction plots for all Models
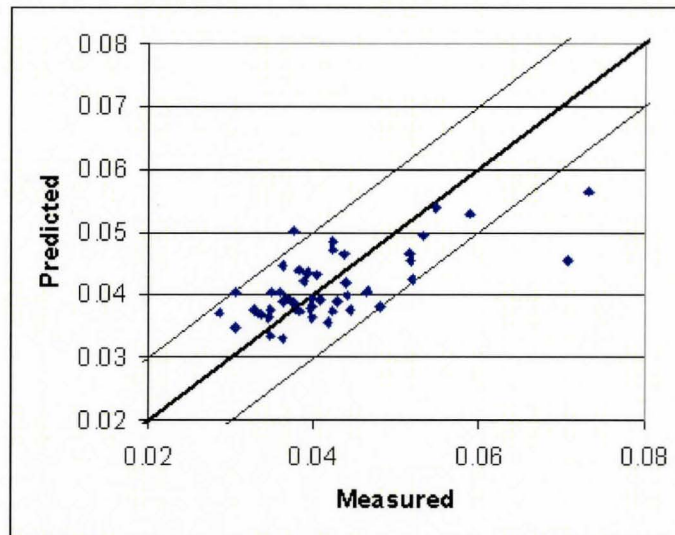
Figure 4.17: Predicted versus measured plot with a 1/y transformation for Model 2 data

4.3.4 Combined Process and Image Data Model

The available process measurements were combined with the image features from Model 2 (the average of the average T1 and T2 and slope) to create a model to predict end-point carbon. The process data included are:

- averages and standard deviations of off-gas chemistry, steam flow, exhaust draft, hood temperature and oxygen flow during the second phase

- values of off-gas chemistry, steam flow, exhaust draft, hood temperature and oxygen flow at the end of the heat

- cumulative sums of off-gas chemistry, steam flow, exhaust draft, hood temperature and oxygen flow for the entire heat

- raw material amounts, chemistry and temperature

- total time of the heat, total heat oxygen, time spent in various parts of the heat

A PLS model was built on the same training and validation datasets used in the previous section. All of the variables described above were incorporated, however, not all of them contributed significantly to the model. All variables where the linear regression coefficient of the PLS model was not statistically different from zero were excluded. This is determined in the Umetrics Simca-P® software, where a 95% confidence interval on the coeffficents is calculated. When the confidence interval includes zero, the variable is excluded. The predicted versus measured plot after all variables were excluded is presented in Figure 4.18. The coefficient plot, which presents the direction and degree in which a variable impacts carbon, is shown in Figure 4.19. The sum of squared prediction error and number of heats where the predicted carbon is outside the +/- 0.01 range are shown in Table 4.8. The parameters show that the process data provides additional information that enhances the carbon prediction, with the value of exhaust draft and hood temperature providing the best information. It is not surprising that most of the process variables that were significant are from the end of the heat, where the largest carbon depletion occurs. Since the carbon

Table 4.8: Parameters for evaluating combined model

Model	No. PLS Comp.	Valid SSE	Valid >0.01	Training >0.01	Total >0.01
Image Model No.2	1	0.873	1/13	3/34	4/47
Combined Model	2	0.696	1/13	1/34	2/47

content did not vary significantly compared to the high error in the measurement, many of the variables were not significant. It is expected that intial chemistry and raw material quantities would be important variables if the BOF was operated to produce steel with a larger range in carbon content.
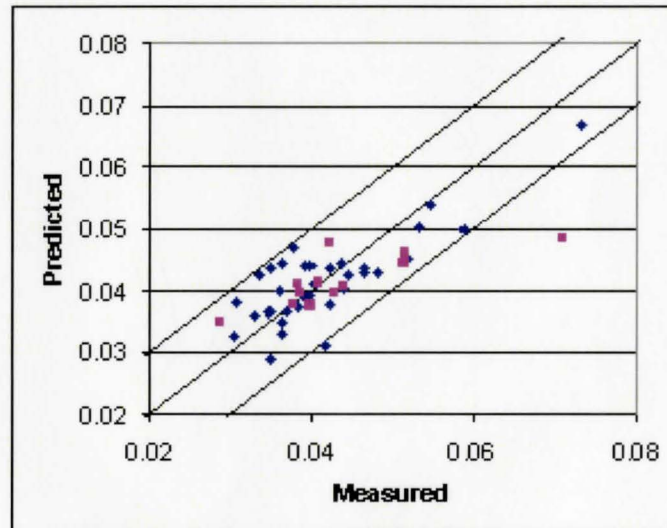

Figure 4.18: Predicted versus measured plot for combined process and image data model
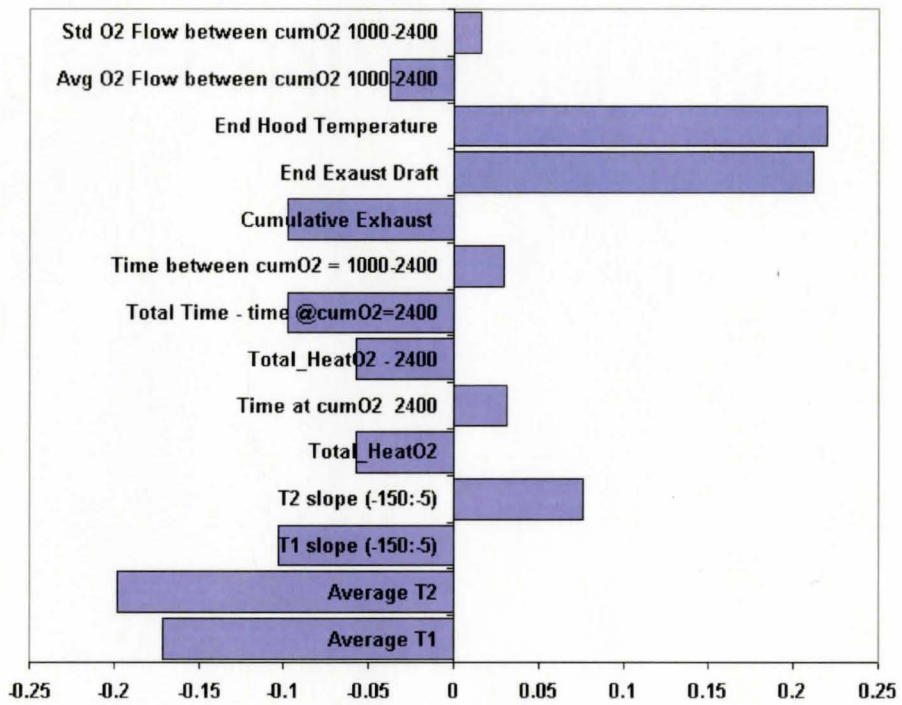
Figure 4.19: Coefficient plot for combined process and image data model

4.4   Online Implementation

Online implementation of the combined image and process data model may be desired. A continuous prediction of carbon can be provided during the last phase of the heat (carbon depletion). This phase would be identified, and then the images for the last 150 values of cumulative oxygen would be used to provide a prediction every 5 values of cumulative oxygen. Process data would also be updated every time a prediction is made. Implementation with missing data would be required and would be completed as discussed in Section 2.2.3. With an online prediction of carbon during the last phase of the heat, the operators would be able to end the heat as soon as the desired end-point is reached.

4.5   Conclusions and Recommendations

The main purpose of a basic oxygen furnace is to reduce the carbon content of hot iron and scrap by injection of oxygen. Lower operational cost is achieved when a heat is terminated just as the carbon content reaches the desired value. In practice, the heat is stopped and a measurement of carbon is taken. An online soft sensor that accurately predicts carbon would save time, oxygen and carbon measurement cost. This chapter was devoted to carbon content prediction using flame images and process data.

A camera was installed to obtain flame images. Although the camera provided excellent images, no camera settings were found that prevented saturation during the middle of the heat and visible images at the end of the heat. Since the most significant carbon depletion occurs at the end of the heat, the camera was configured to obtain the best images at the end of a heat.

Image pre-processing was performed to address the changing field of view of the camera. Build-up on the top of the vessel and furnace as well as slightly different angle vessels resulted in the different field of view. Standard edge detection techniques were used to identify the vessel edge to obtain windowed images with similar number of vessel and flame

pixels within a heat and between subsequent heats.

Features were extracted from the images of the last 120 seconds of a heat. The average T1 and T2 approach as well as the mask method were used to extract features from the images. Several PLS models were built with the features to predict the final carbon content, with both traditional batch and data characterization methods. The model with the best prediction capability uses the average value of T1 and T2 and the slope of T1 and T2 from 5 to 150 units of cumulative oxygen from the end of the heat. Several non-linear transformations were also applied to the carbon measurement in an attempt to improve prediction for high carbon heats, with significant improvement.

Image data features and process data were then combined in another PLS model. This model presented excellent prediction with only 2 of the 47 heats (4.3%) not being predicted within the desired range of +/- 0.01% carbon.

Online implementation of the combined image and process data model for carbon prediction will be investigated once the plant resumes operation from an extended inventory outage. Another possibility is to analyze the use of flame images to predict the final temperature.

4.6 Acknowledgments

Chapter 5

Coal-fired Boiler

This chapter provides details on the experiments and results obtained to date at the OPG-Atikokan coal-fired power generation plant.

5.1 Introduction

Coal is used for approximately 40 percent of the world's electricity generation, due to it's abundancy in nature and high energy content (World Coal Institute [2007]). However, burning coal also releases harmful greenhouse gases. Growing concerns over global warming have led to research for alternate fuel sources in developed countries. Many types of biomass (wood, straw, sewage) have been studied for cofiring with coal as a means to reduce emissions, with over 100 trials in 16 different countries having been performed in recent years (Baxter [2005]). There are important considerations that need to be assessed to convert to a full-biomass or cofired energy production scheme such as the boiler efficiency, boiler stability, the amount and chemistry of the produced ash, boiler fouling, capital cost required and cost of the biomass (Pronobis [2006]). A Canadian study funded by the Ministry of Environment through Ontario Centres of Excellence aims to look into the conversion of Ontario Power Generation's Atikokan boiler from coal to biomass. McMaster University's

involvement encompasses the use of images and process data to study boiler stability and energy efficiency.

As of October 2008, analysis of experiments performed to establish a coal-only baseline have been completed. Progress on biomass trials has been hampered by a 6-month maintenance outage experienced by the plant. These trials are planned for the last week of November 2008, and the analysis will be completed outside this thesis. Coal-only imaging results are provided in this chapter.

5.1.1 Process Description

A coal-fired boiler crushed coal is burned and water is converted to steam in tube banks situated in the boiler walls. The generated steam is sent to a steam turbine to produce electricity. A plant diagram is shown in Appendix B. The particular boiler studied in this work has 5 burner banks, located at different heights and faces of the boiler, where coal and air are injected. Each burner bank has 3 individual burners, and the air to fuel ratio for the entire bank is controlled. A varying number of burners banks and combinations are engaged depending on the energy requirements. (Atikokan Generating Station [2008])

5.1.2 Camera Installation

As part of this project,three new cameras were installed at various locations in the boiler. This was required as the current cameras installed were analogue and of poor quality. Operators use these cameras only to ensure a flame is present. The cameras have automatic gain adjustment, making the images brighter when the load is lower. It would be difficult to perform a multivariate analysis using these images.

Three exiting view ports were selected for camera installation. Figure 5.1 presents a sketch of these locations and their view of the burners banks. The two top cameras (8S and 8N), contain the burners on the opposite wall in their field of view. The camera directly above burner bank 2 has a view of burner levels 2 and 3. This camera was installed to

have a better view of a specific burner level, as other partners involved in this project have instrumentation installed on this burner bank. An analysis combining various partner's measurements is to be completed outside this thesis.
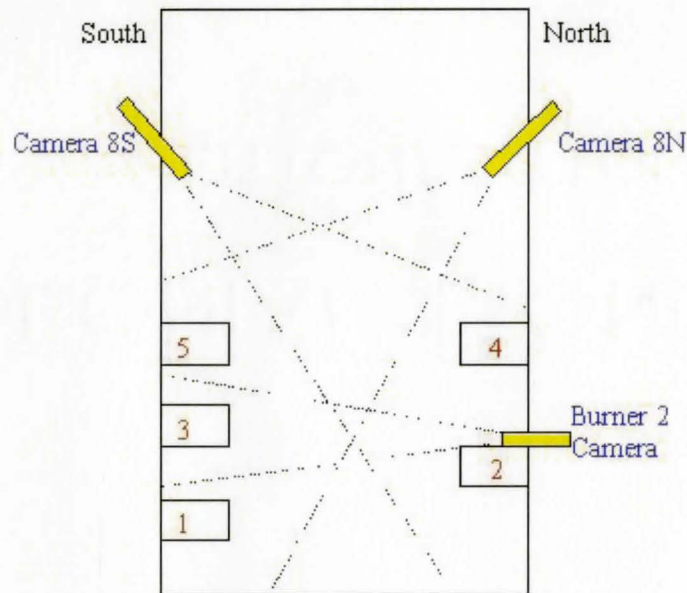
Figure 5.1: Sketch of camera locations and field of view

JM Canty Ⓡ high temperature cameras (JM Canty Inc. [2008]) were selected for this project because they have several advantages over competitors including:

- Lower cost

- Air cooling instead of water cooling:

  - Decreases maintenance

  - Safer in case of a leak in combustion processes

- Protection of electronics with fused glass, most competitors have limited protection

- Digital, with easy to use software for video /frame recording

Figure 5.2 presents a sketch of the camera and mounting locations prepared at the plant. The plate is removable and the camera is inserted into place.
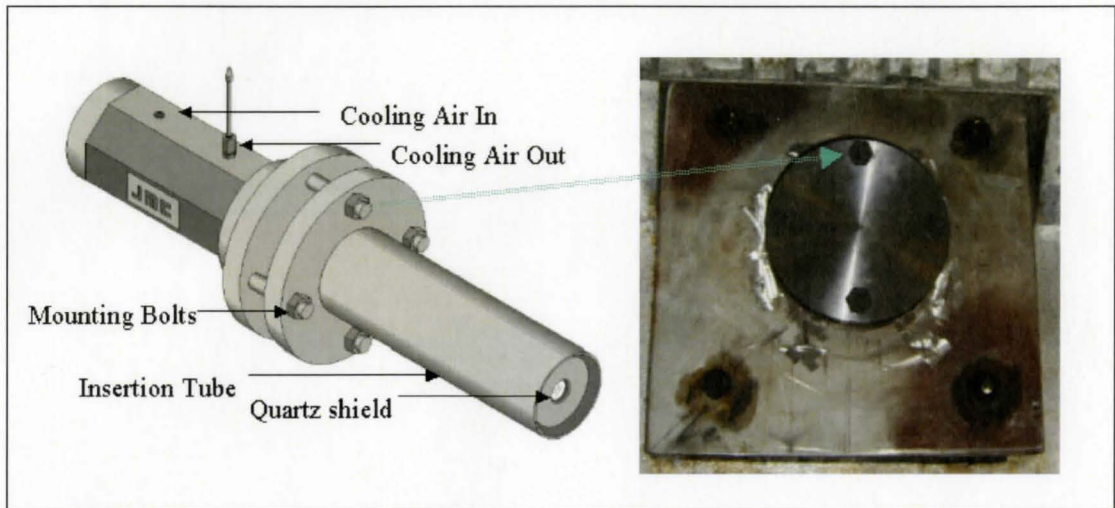
Figure 5.2: Sketch of camera(JM Canty Inc. [2008]) and mounting location at the boiler

5.1.3 Description of Coal-only experiments

In order to establish a coal-only baseline, a two-day experiment was performed at the plant. Various air to fuel ratios and load experiments (energy production) were completed. The air to fuel ratios were selected based on plant safety restrictions and by keeping all partners of the project in mind. Some partners were interested in monitoring the whole boiler, while other partners had equipment installed on just one burner bank (burner level 2). The air to fuel ratios were thus varied for the boiler as a whole and also just for burner 2. Tables 5.1 through 5.4 present the 1 hour experiments operated at the various loads. A + sign indicates a higher than optimal air to fuel ratio, a - sign indicates a lower than optimal air to fuel ratio, and 0 represents the optimal air to fuel ratio.

Table 5.1: Boiler experiments performed at full load

TestID	L1	L2	L3	L4	L5
101-7:00	0	0	0	off	0
102-8:00	+	+	+	off	+
103-9:00	0	0	0	off	0
104-10:00	++	++	++	off	++
105-11:00	0	0	0	off	0
106-12:00	0	-	+	off	0
107-13:00	0	+	-	off	0

Table 5.2: Boiler experiments performed at half load

TestID	L1	L2	L3	L4	L5
201-15:00	0	0	0	off	off
202-16:00	+	+	+	off	off
203-17:00	0	0	0	off	off
204-18:00	-	-	-	off	off
205-19:00	0	0	0	off	off
206-20:00	0	-	+	off	off
207-21:00	0	+	-	off	off

Table 5.3: Boiler experiments performed at minimum load with burner 1 and 2

TestID	L1	L2	L3	L4	L5
301-7:00	0	0	off	off	off
302-8:00	+	+	off	off	off
303-9:00	0	0	off	off	off
304-10:00	-	-	off	off	off
305-11:00	0	0	off	off	off
306-12:00	+	-	off	off	off
307-13:00	-	+	off	off	off

Table 5.4: Boiler experiments performed at minimum load with burner 2 and 3, and natural gas ignitors for 404-407

TestID	L1	L2	L3	L4	L5
401-14:00	off	0	0	off	off
402-15:00	off	-	+	off	off
403-16:00	off	+	-	off	off
404-17:00	off	0	0	off	off
405-18:00	off	-	+	off	off
406-19:00	off	+	-	off	off
407-20:00	off	0	0	off	off

5.2 Results and Discussion

5.2.1 Camera Images

Several challenges associated with the installed cameras were experienced throughout the experiments. The two top cameras (8S and 8N) experienced some pitting in the protective quartz shield (shown in the camera diagram, Figure 5.2) of the camera. This occurred between the the time of the camera installation and the time when the experiments were preformed. During soot-blowing, which is when steam is blown at the walls to remove any build-up that may have accumulated, portions of the build-up hit the camera shield and cause the pitting. No increase in pitting occurred over the 2-day experiment, thus the pits did not impact the analysis. A solution to prevent further pitting is being developed by the manufacturer.

The camera field of view becomes obstructed by build-up on the walls surrounding the camera insertion. This, as well as the pitting can be seen in Figure 5.3. The changing field of view introduces complexity as there is no physical hardware solution for this, and must be dealt with in the analysis. There are several methods that could be employed to handle this, including masking the build-up and only utilizing the remaining pixels for the analysis.

However, this introduces non-linearities as there would be a varying amount of edge pixels depending on the shape of the build-up. A simple window technique was employed, where only the camera pixels that were never covered by build-up are used for analysis. This is shown in Figure 5.4.
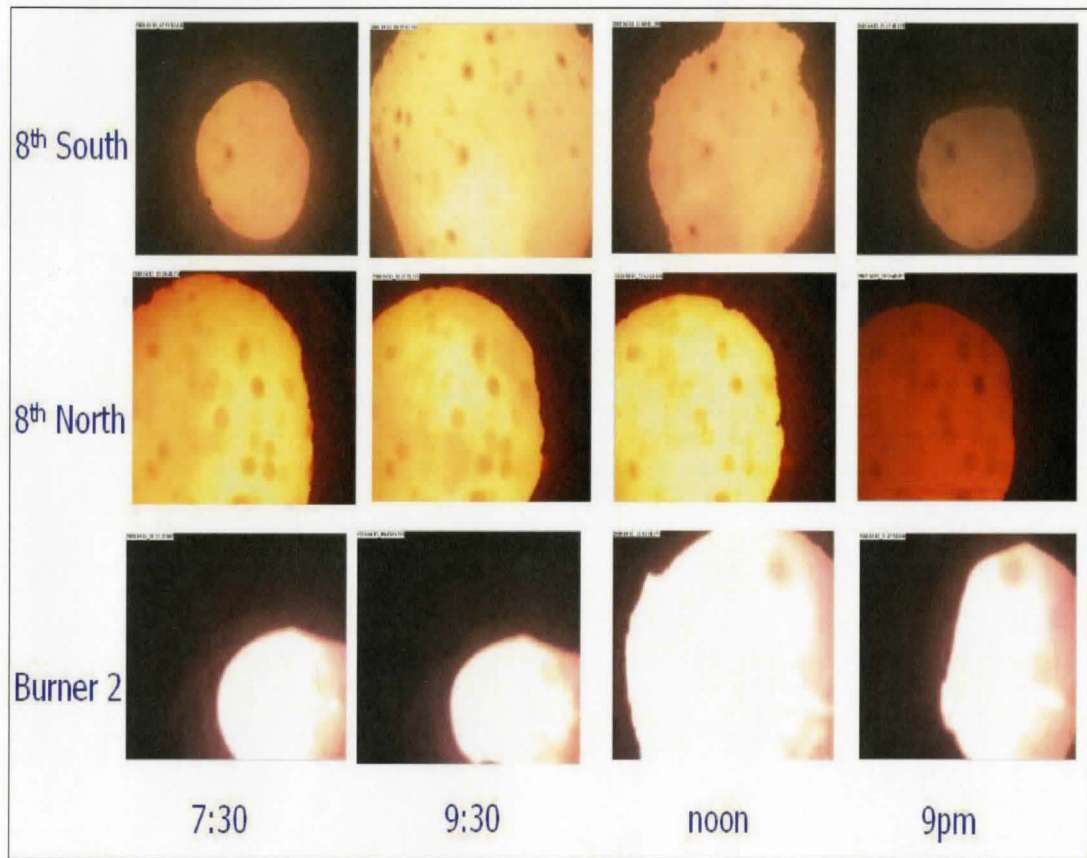

Figure 5.3: Camera Images: demonstration of pitting and build-up over time
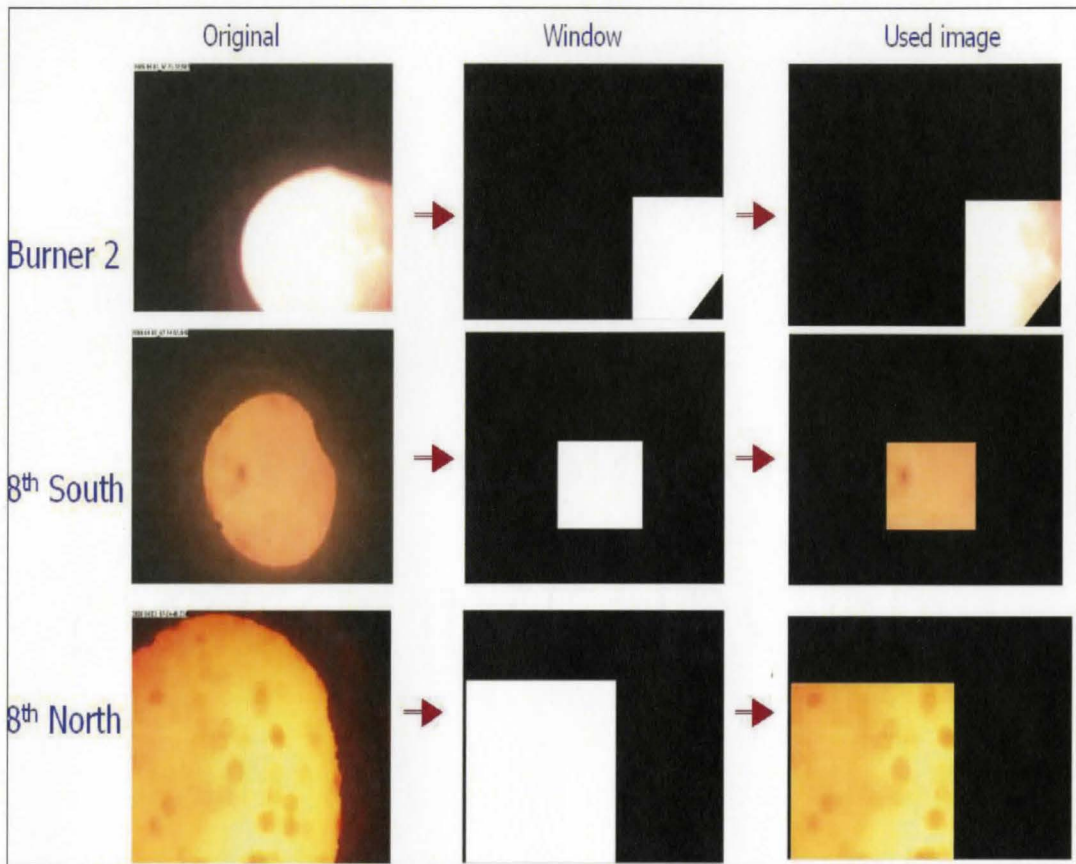
Figure 5.4: Window technique for excluding build-up pixels

5.2.2 Build-Up Monitoring

The challenge of the changing field of view discussed in Section 5.2.1 also presents an opportunity to monitor build-up in the sections of the boiler where the cameras are installed. Build-up is a large problem in these boilers, and is of special concern when using biomass, which is expected to lead to more fouling (Pronobis [2006]). The ability to identify fouling rates is critical.

To determine the amount of build-up in the field of view of a specific camera, a mask is identified in the T1T2 score image that encompasses the build-up pixels. Figure 5.5 presents this method for the burner 2 camera. The mask is applied to all of the images, and the
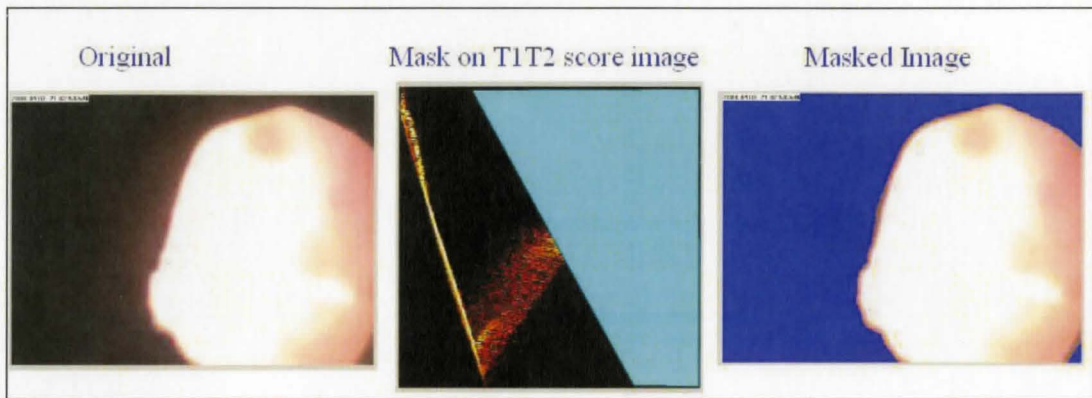
Figure 5.5: Burner 2 build-up mask and application to an image
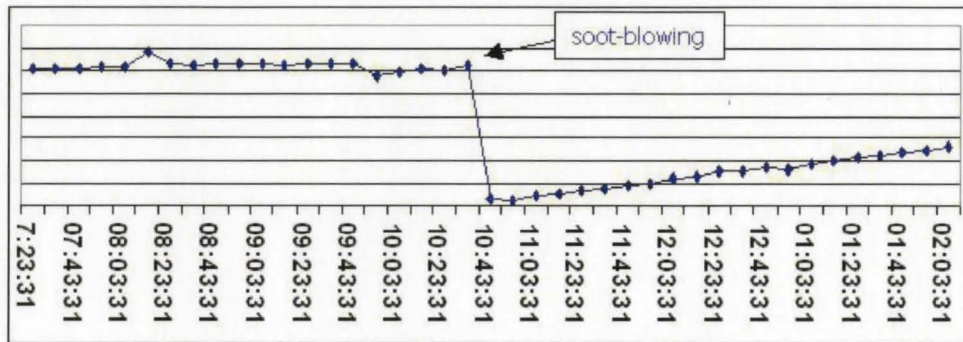
Figure 5.6: Burner 2 camera build-up during full load experiments

number of pixels falling under the mask are used as a measure of fouling. Figure 5.6 shows this measurement over time for the burner 2 camera during the full load experiments. The fouling was cleared away using soot-blowing and then built up again over time. The speed at which fouling occurs at different loads could be an interesting parameter to monitor and compare between coal and biomass operation.

5.2.3 Analysis at varying loads

This section presents the analysis performed for the various experiments. It is trivial to distinguish between the four different groups of experiments, as the glow inside the boiler is much brighter for higher loads. The goal is to be able to distinguish between the different air to fuel ratio experiments performed at each load.

Six images every hour are used from each camera for the duration of a set of experiments. A model was built using the method described in Section 2.3, where the overall $X^T X$ matrix for all of the images from one camera (windowed to remove build-up) was calculated and a PCA model was built. Score images are produced by scaling with the minimum and maximum of the scores over all the images (also described in Section 2.3) and features are then extracted from the score images. In this case, the features used were 32x32 masks from the score image (size is 256 by 256), as illustrated in Figure 5.7. Thus, from each image, 64 features are extracted.
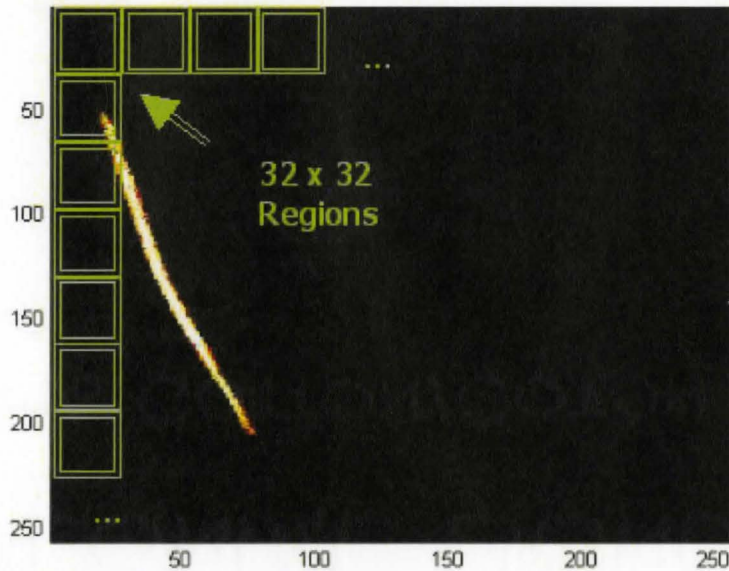

Figure 5.7: Feature Extraction: 32x32 masks extracted from a score image

The extracted features are used for model building for each group of experiments. A PCA

model is created to determine whether the different air to fuel ratio experiments can be distinguished by the camera. PLS models are also built in an attempt to predict energy efficiency and total air to fuel ratio.

Full Load Experiments (from Table 5.1)

The results of the PCA model for each camera are shown in the score plots in Figure 5.8. Repeat experiments are expected to have similar features and thus be located in a similar location on the score plot. However, this did not occur, as seen in Figure 5.8. Only burner 2 showed some of the expected clustering. A PCA model finds the directions of most variance in a dataset, and these results clearly show that there are other sources of variation in the process that are unrelated to the experiments performed. As highlighted in Figure 5.8, it is likely that time is this source of variation. An analysis on the process data completed by ProSensus Inc. also showed that the main source of variation was time (see Figure 5.9). The process probably never reached steady state during the experiments.

A PLS model was created for each camera to try and relate the image features to energy efficiency (EE) and total air to fuel ratio (TAF). These models could find features of the image that relate to these two important parameters, even if they aren't the greatest source of variation in the data. However, as can be seen in Figure 5.10, the prediction is poor (low R^2 and Q^2) for camera 8S. R^2 is a measure of how much of the variation in the Y variable is modeled, and Q^2 is the expected performance on a testing dataset, determined by cross-validation. The results of the other two cameras are similar.

The results for the remaining groups of experiments are equally poor. Figures 5.11,5.12, and 5.13 show the score plots for each camera at these loads. PLS models are not presented as they are not able to predict energy efficiency or total air to fuel ratio.
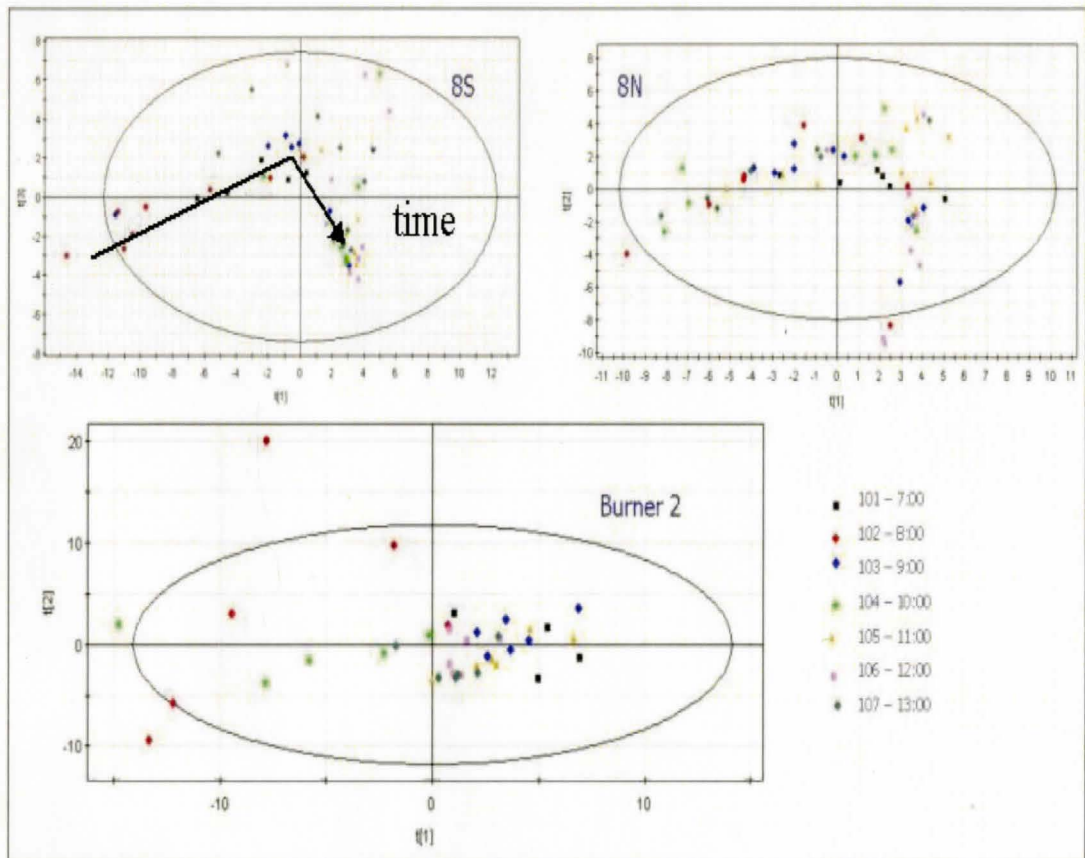
Figure 5.8: Score plots for PCA models for the three cameras for the full load experiments
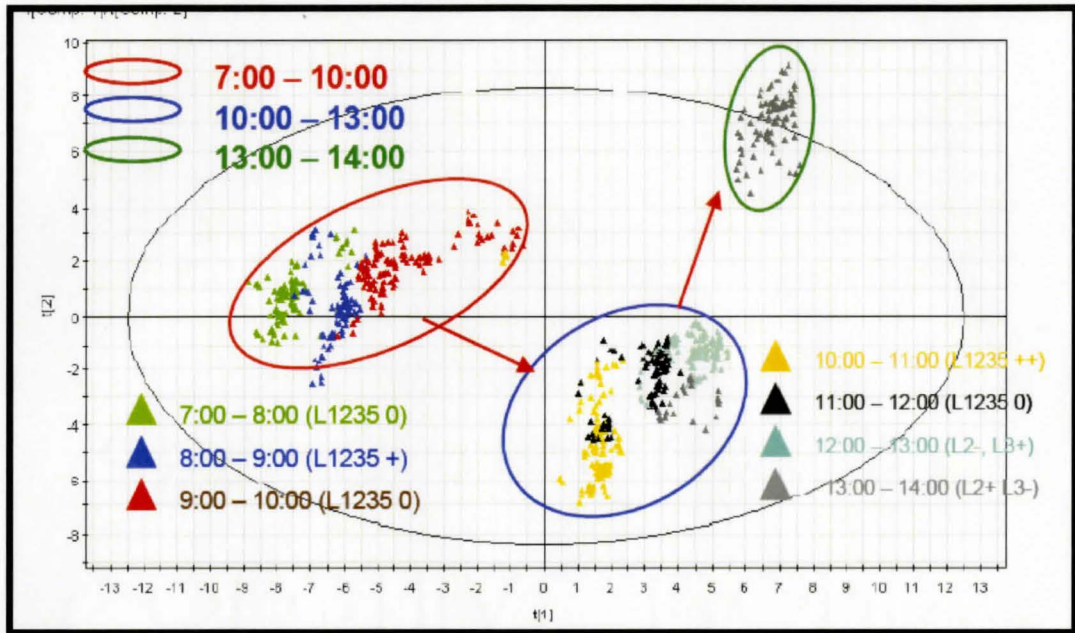
Figure 5.9: Score plot of process data during the full load experiments (analysis by ProSensus Inc.)

Figure 5.10: PLS model predictions at full load for camera 8S

Figure 5.11: Score plots for PCA models for the three cameras for the half load experiments

Figure 5.12: Score plots for PCA models for the three cameras for the minimum load experiments using Burner 1 and 2

Figure 5.13: Score plots for PCA models for the three cameras for the minimum load experiments using Burner 2 and 3
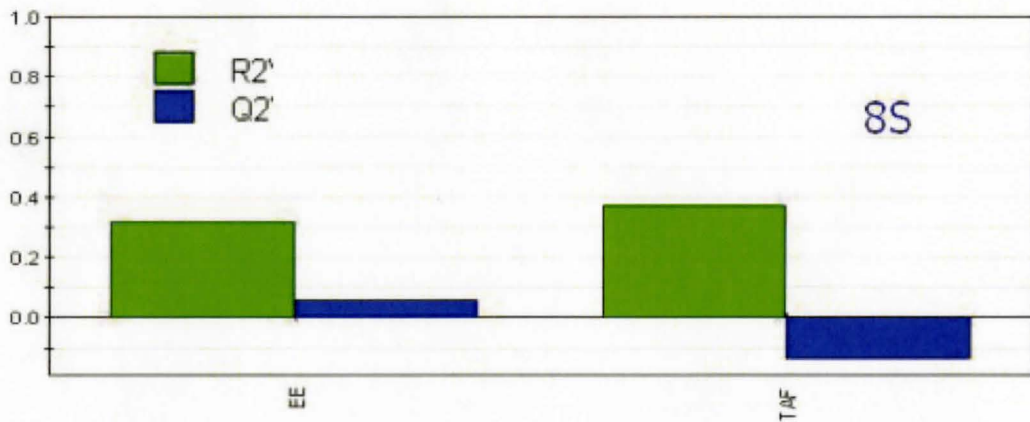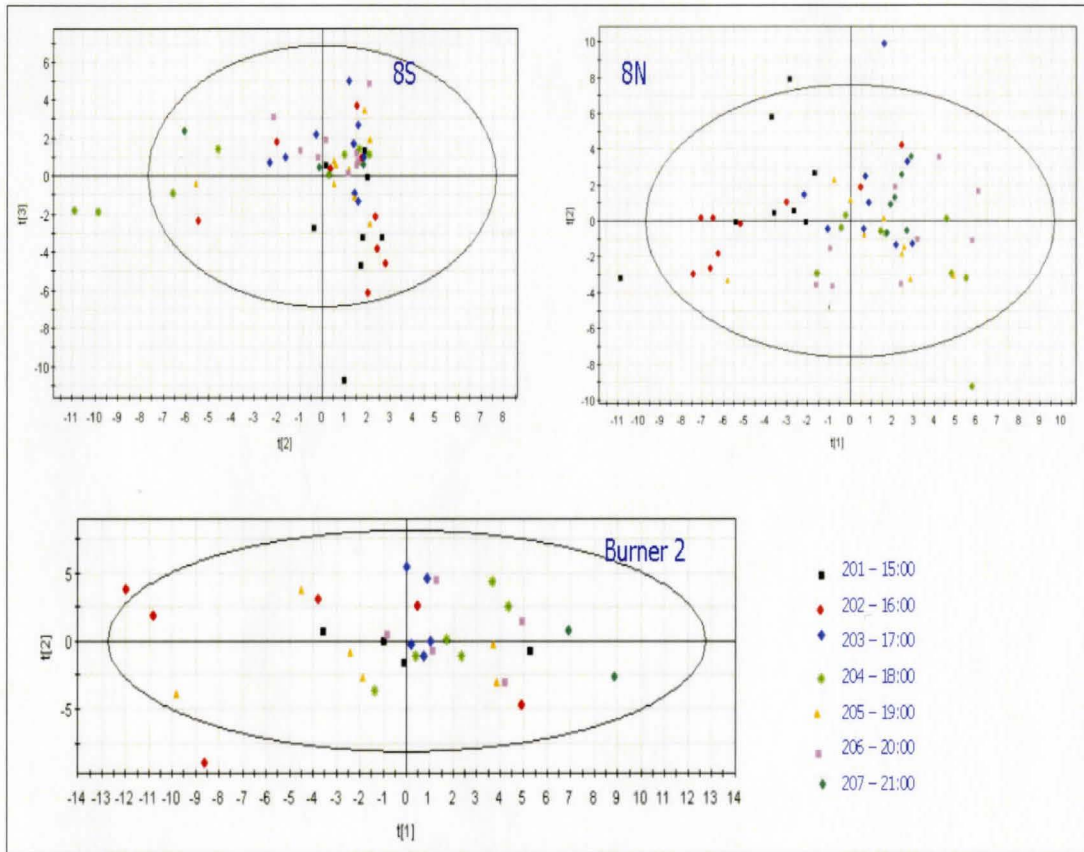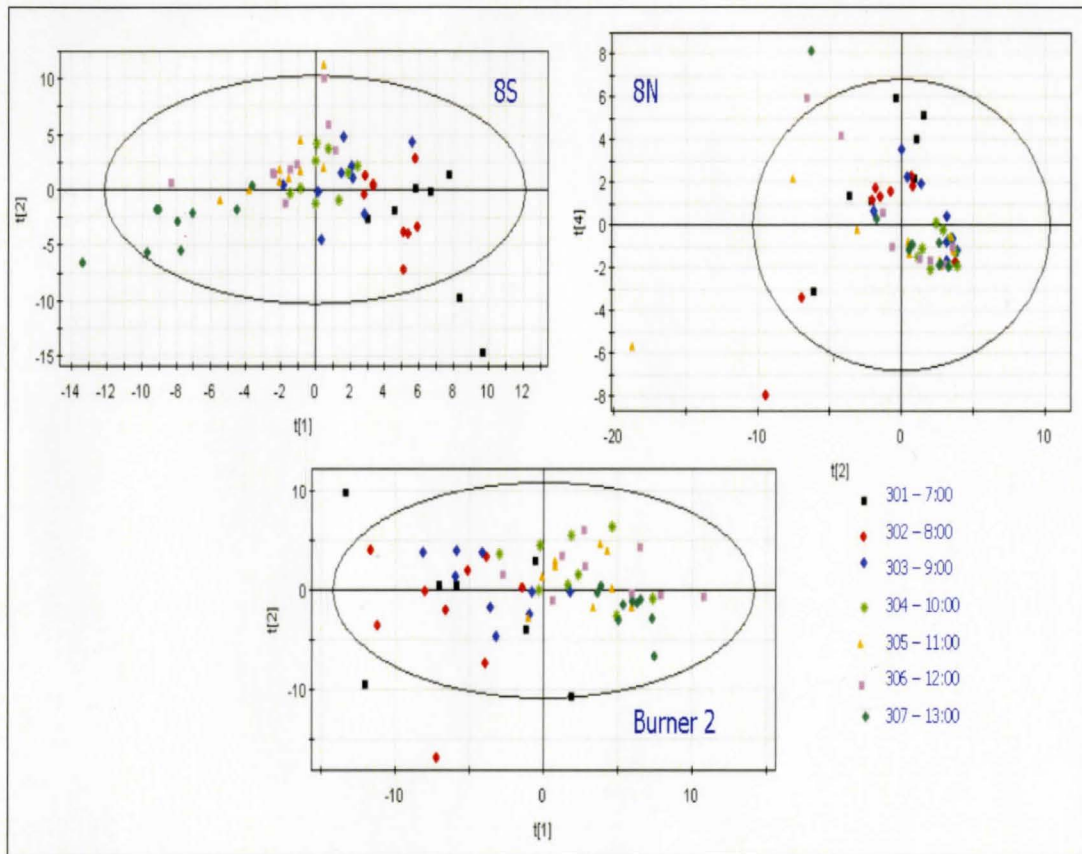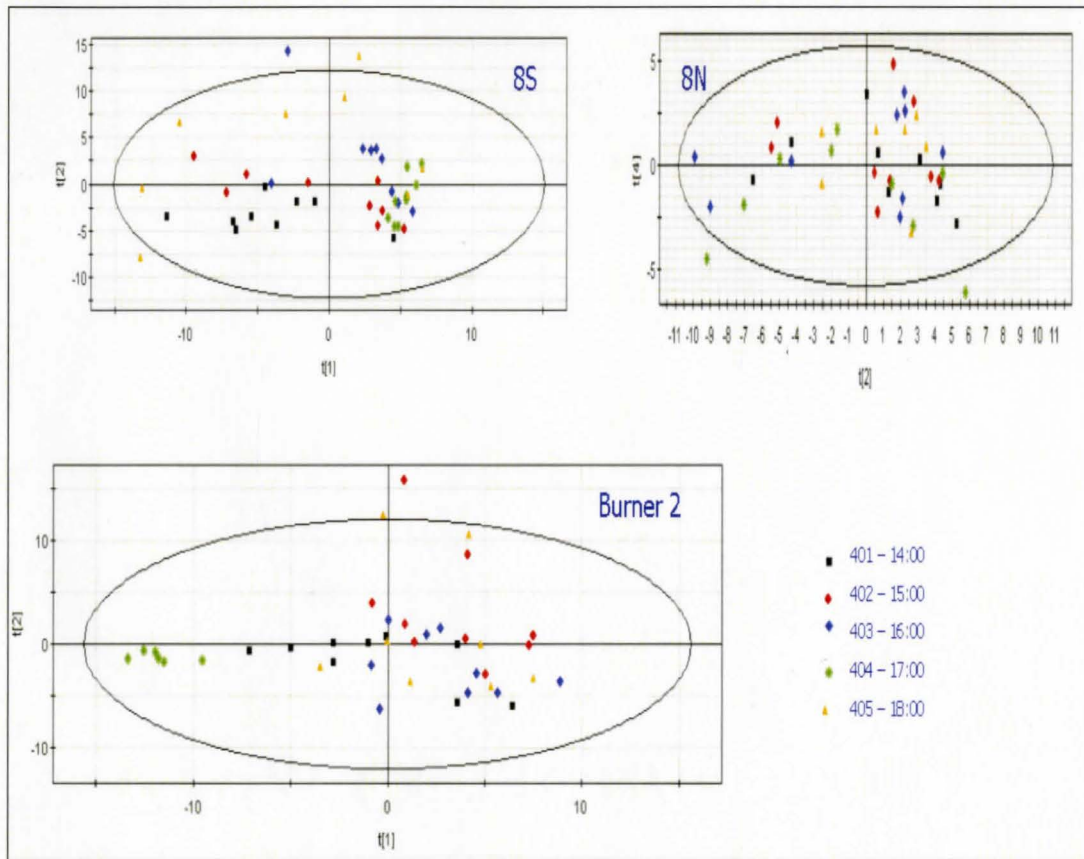
5.3 Conclusions and Future Work

Conclusions

Three cameras were successfully installed to have a view of all burner banks, with one camera having a concentrated view on burner bank level 3. Pitting of the protective quartz shields of the cameras did occur but did not impact the experimental analysis. A mechanical fix will be implemented.

Several coal-only experiments were performed over a two day period. Energy production levels and air to fuel ratios were varied in 1 hour experiments. The goal was to be able to distinguish between the various air to fuel ratios at each production level. Operating a burner at the optimal air to fuel ratio results in the most efficient combustion. An online prediction of this metric from the cameras would be ideal.

It was found that the images did not contain sufficient information to be able to predict air to fuel ratio. Repeat experiments did not show similar image characteristics, and images within a specific experiment often contained very different features. It may be that the process was never at steady-state throughout the experiments. Although a change in air-to fuel ratio impacts off-gas chemistry within five minutes, it may be that major production level changes do not settle so quickly. Signal to noise ratio may be another reason for these suboptimal results. The air to fuel ratio may not have been varied enough. In any future experiments, such as the biomass experiments, less load changes will be made with more significant variations in the air to fuel ratios in hopes of obtaining better results.

An important finding is that fouling at the camera locations can be determined from the images through a simple masking technique. This is significant because fouling is of major concern when charging biomass, and the ability to have some monitoring points is key.

Future Work

There is significant future work that exists in this project that will be performed beyond the completion of this thesis. This includes analyzing several months of coal-only process data and completion of biomass trials.

5.4 Acknowledgments

Chapter 6

Conclusions and Recommendations

High energy costs, stricter environmental regulations and a high Canadian dollar have led Canadian manufacturers to find new ways to improve energy efficiency in their processes. Combustion processes, which are especially hard hit by these changes, were studied in this work. Multivariate image and process data analysis was applied to three combustion processes: a lime kiln, a basic oxygen furnace, and a coal-fired boiler. The conclusions and recommendations are summarized for each case study separately.

Lime-Kiln Analysis

The primary goal for this analysis was to create a multivariate model to predict final product temperature several hours into the future for possible use in a supervisory system or closed-loop control system. To build a successful model, both images and process data were required. 12 masks were identified from the images that provided important information for temperature prediction up to 2 hours into the future. However, transition periods (when the process was between steady-state values) were not well captured by an image only model, thus process data were also incorporated into the model. Dynamic information was captured using first-order plus deadtime filters of both the images and the process data to project process conditions at a current time into the future. These new parameters were

then used to build PLS models 1 hour and 2 hours into the future to predict final product temperature. The 1 hour model provides very good prediction results, while the 2 hour model provided reasonable results with some delay during transition periods. Future work includes placing both the 1 hour and 2 hour models online and potential use for online control.

Basic Oxygen Furnace

The goal of the basic oxygen furnace analysis was to predict end-point carbon of the batch process. An online prediction of carbon could help the operators end the batch as soon as the desired carbon is reached, limiting oxygen consumption and reducing operational costs. To adequately use the images of a newly installed camera, traditional image analysis was used to stabilize the field of view throughout a heat and between all heats. Features were extracted from the new flame images and used for carbon prediction. The best image features were found to be average score values of the images. A successful carbon prediction model was then built by combining these image features and available process data. Future work includes placing the model online and improvement of the model for high carbon heats.

Coal-Fired Boiler

The goal of this work was to use image analysis to study flame stability and energy efficiency under various loads and air to fuel ratios. Three cameras were installed and the flame images for a set of designed experiments were studied. It was difficult to predict energy efficiency and monitor flame stability as the process never reached steady state during the experiments. An unexpected result was that the cameras can be used to monitor localized fouling, which could be very important as the plant moves towards co-fired steam production using both coal and biomass. Future work will include performing biomass experiments and analyzing these results, as well as studying several months of coal-only operation to determine areas of improvement.

This thesis has shown that the use of multivariate analysis of flame images and process data in combustion process is very promising. A high-temperature manufacturing unit should benefit from such an analysis if stable flame images can be obtained.

List of References

ARTEAGA, F. AND FERRER, A. (2002). Dealing with Missing data in MSPC: several methods for different interpetations, some examples. *Journal of Chemometrics*, **16**, 408–418.

ATIKOKAN GENERATING STATION (2008). *Atikokan Generating Station: Information Brochure, available at* `www.opg.com/power/fossil/atikokan.asp` .

BAXTER, L. (2005). Biomass-coal co-combustion: opportunity for affordablee renewable energy . *FUEL*, **84**, 1295–1302.

BHARATI, M. (2002). *Multivariate Image Analysis and Regression for Industrial Process Monitoring and Product Quality Control*. PhD Thesis, Department of Chemical Engineering, McMaster University, Canada.

BHARATI, M. AND MACGREGOR, J. F. (1997). Softwood Lumber Grading through On-line Multivariate Image Analysis Techniques . *International Statistical Review*, **65**, 309–323.

BHARATI, M. AND MACGREGOR, J. F. (1998). Multivariate Image Analysis for Real-Time Process Monitoring and Control. *Industrial and Engineering Chemistry Research*, **37**, 4715.

BOATENG, A. A. (2008). *Rotary Kilns: Transport Phenomena and Transport Processes*. Elsevier.

BRUWER, M. J. (2006). *Process Systems Approaches to Diagnostic Imaging And Identification*. PhD Thesis, Department of Chemical Engineering, McMaster University, Canada.

BURNHAM, A. J., VIVEROS, R., AND MACGREGOR, J. F. (1996). Frameworks for Latent Variable Multivariate Regression. *Journal of Chemometrics*, **10**, 31–45.

CHAMPAGNE, M. AND DUDZIC, M. (2002). Industrial use of multivariate statistical analysis for process monitoring and control. In *American Control Conference, 2002. Proceedings of the 2002*, pp. 594–599, Anchorage, AK. AACC.

DUDZIC, M. AND QUINN, S. (2002). Predictive modeling using adaptive PLS desulphurization reagent control system. In *American Control Conference, 2002. Proceedings of the 2002*, pp. 604–605, Anchorage, AK. AACC.

DUDZIC, M., VACULIK, V., AND MILETIC, I. (1999). Applications of multivariate statistics at Dofasco. In *Advanced Process Control Applications for Industry Workshop*, pp. 27–29.

ERIKSSON, L., JOHANSSON, E., N.KATTANEH-WOLD, TRYGG, J., WIKSTROM, C., AND WOLD, S. (2006). *Multi- and Megavariate Data Analysis, Part 1, Basic Principles and Applications*. Umetrics Academy.

GELADI, P. AND KOWALSKI, B. (1986). Paritial Least Squares Regression: A Tutorial . *Analytica Chimica*, **185**, 1–17.

GLASBEY, C. AND HORGAN, G. (1995). *Image Analysis for the Niological Sciences*. John Wiley and Sons.

GOODARZI, F. (2006). The rates of emissions of fine particles from some Canadian coal-fired power plants . *FUEL*, **85**, 425–433.

HERAEUS ELECTRO NITE (2009). *QuiKTap TimeSaver Sensor, information available at* www.electronite.de/eng/Products/sensors/SteelQuiKTap.html .

JM CANTY INC. (2008). *UltraTemp High Temperature Cameras available at* www.jmcanty.com/Products/TempCameraTemperatureMeasurement/index.html .

KASSIDAS, A. AND MACGREGOR, J. F. (1998). Synchronization of Batch Trajectories using Dynamic Time Warping. *AIChE Journal*, **44**, 864–875.

KRESTA, J. V., MARLIN, T. E., AND MACGREGOR, J. F. (1994). Development of Inferential Process Models Using PLS . *Computers and Chemical Engineering*, **18**, 597–611.

MACGREGOR, J. F. (2003a). Data-Based Methods for Process Analysis, Monitoring and Control. In *Proceedings of IFAC System Identification*, pp. 1–10, Rotterdam, August.

MACGREGOR, J. F. (2003b). Using On-Line Process Data to Improve Quality: Challenges for Statisticians . *Industrial and Engineering Chemistry Research*, **42**, 5345–5353.

MACGREGOR, J. F. AND KOURTI, T. (1999). Multivariate Statistical Treatment of Historical Data for Productivity and Quality Improvements. In Joseph F. Pekny, Gary E. Blau, B. C. E. (Ed.), *AIChE Symposium Series No. 320, Vol 94*, pp. 31–41. CACHE and AICHE.

MARLIN, T. E. (2000). *Process Control - Designing Processes and Control Systems for Dynamic Performance, 2nd Edition*. McGraw Hill.

NELSON, P. R. C., TAYLOR, P. A., AND MACGREGOR, J. F. (1996). Missing data methods in PCA and PLS: Score Calculations with incomplete observations. *Chemometrics and Intelligent Laboratory Systems*, **35**, 45–65.

NOMIKOS, P. AND MACGREGOR, J. F. (1994). Monitoring of Batch Processes using Multiway Principal Component Analysis. *AIChE Journal*, **40**, 1364–1375.

PRONOBIS, M. (2006). The influence of biomass co-combustion on boiler fouling and efficiency . *FUEL*, **85**, 474–480.

PROSENSUS INC. (2007). *Multivariate Methods for Process Analysis, Monitoring and Quality Improvements : An Intensive Course.*

QUADTEK MIRION (2008). *Quadtek M554 Spyrometer Datasheet, available at* www.mirion.com/en/products/datasheets/is/M554.pdf .

SZATVANYI, G. AND DUCHESNE, C. (2006). Multivariate Image Analysis of Flames for Product Quality and Combustion Control in Rotary Kilns. *Industrial and Engineering Chemistry Research*, **45**, 4706–4715.

WESTERHUIS, J., KOURTI, T., AND MACGREGOR, J. F. (1999). Comparing Alternative Approaches for Multivariate Statistical Analysis of Batch Process Data. *Journal of Chemometrics*, **13**, 397–413.

WORLD COAL INSTITUTE (2007). *Coal Facts 2007, from* `www.worldcoal.org`.

YU, H. (2003). *Development of Vision-Based Inferential Sensors for Process Monitoring and Control.* PhD Thesis, Department of Chemical Engineering, McMaster University, Canada.

YU, H. AND MACGREGOR, J. F. (2003a). Digital Imaging for Process Monitoring and Control with Industrial Applications. In *Proceedings of IFAC ADCHEM'03*, Hong Kong.

YU, H. AND MACGREGOR, J. F. (2003b). Multivariate Image Analysis and Regression for Prediction of Coating Content and Distribution in the Production of Snack Foods. *Chemometrics and Intelligent Laboratory Systems*, **67**(2), 125–144.

YU, H. AND MACGREGOR, J. F. (2004). Monitoring Flames in an Industrial Boiler Using Multivariate Image Analysis. *AIChE Journal*, **50**(7), 1474–1483.

Appendix A

NIPALS algorithm

This Appendix provides the NIPALS algorithm for PCA, and PLS and a discussion on incorporating missing data. More information can be found in the following references: Kresta *et al.* [1994] and Geladi and Kowalski [1986] and Eriksson *et al.* [2006].

NIPALS for PCA

1. Select a non-zero column of X and set this equal to t

2. Project X onto t to find the loading p: $p = X^T t \ / \ t^T t$

3. Normalize p (loading vector) to unit length: $p = p \ / \ \|p\|$

4. Calculate the score vector: $t = Xp \ / \ p^T p$

5. Check for convergence : if t from step 1 and t from step 4 are different by more than a defined threshold, return to step 2

6. Once convergence has been reached, calculate the error: $E = X\text{-}tp^T$

7. If another component is required start at step 1, with X = E (the deflated matrix)

Incorporating missing data into PCA Algorithm

To incorporate missing data into the NIPALS algorithm, the following changes are made to the steps above:

1. Select a non-zero column of X and set this equal to t. The column should contain no missing data.

2. To find the loading vector p, each entry of the vector is calculated separatley. X observations in each column that are missing are ignored. 3. Normalize p (loading vector) to unit length. Use only the number of non-missing observations in each column for this step. 4. Calculate the score vector one observation at a time, excluding columns where there is missing data. 5. No change to this step. 6. Once convergence has been reached, calculate the error: $E = X\text{-}tp^T$. Missing data entries will continue to be missing.

7. If another component is required start at step 1, with $X = E$ (the deflated matrix)

NIPALS for PLS

1. Select a non-zero column of X and set this equal to w. Normailize to length 1.

2. Calculate the score vector t: $t = Xw$

3. Calculate the Y loading vector q: $q = Y^T t$

4. Calculate new weight vector w: $w = X^T t$

5. Check for conergence: if w from step 1 and w from step 4 are different by more than a defined threshold, return to step 2

6. Once convergence has been reached, calculate the loading vector p: $p = X^T t / t^T t$

7. Calculate the error on X: $Ex = X\text{-}tp^T$

8. Compute the regression of Y onto t: $c = Y^T t / t^T t$

9. Calculate the error on Y: $Ey = Y\text{-}t^*c^T$

10. If another component is required start at step 1, with $X = Ex$ and $Y = Ey$ (the deflated matrices)

Incorporating missing data into PLS Algorithm

To incorporate missing data into the PLS NIPALS algorithm, the following changes are made to the steps above:

1. Select a non-zero column of X and set this equal to w. Normailize to length 1. The

column should contain no missing data.

2. Calculate the score vector t: t = Xw one observation at a time, excluding columns where the data are missing.

3. Calculate the Y loading vector q: $q=Y^T t$

4. Calculate new weight vector w one column at a time, excluding rows where data are missing

5. Check for convergence: if w from step 1 and w from step 4 are different by more than a defined threshold, return to step 2

6. Once convergence has been reached, calculate the loading vector p one column at a time, excluding rows with missing data 7. Calculate the error on X: $Ex = X-tp^T$

8. Compute the regression of Y onto t: $c= Y^T t / t^T t$

9. Calculate the error on Y: $Ey = Y-t*c^T$

10. If another component is required start at step 1, with X = Ex and Y=Ey (the deflated matrices)

Glossary

X: the data matrix

Y: the response data matrix

t: the score vector

p: the loading vector

Ex: the deflated X matrix

Ey: the deflated Y matrix

q: the Y loading vector for PLS

w: PLS X loading vector

c: regression coefficient of Y on t

Appendix B

Coal-Fired Electricity Plant Diagram

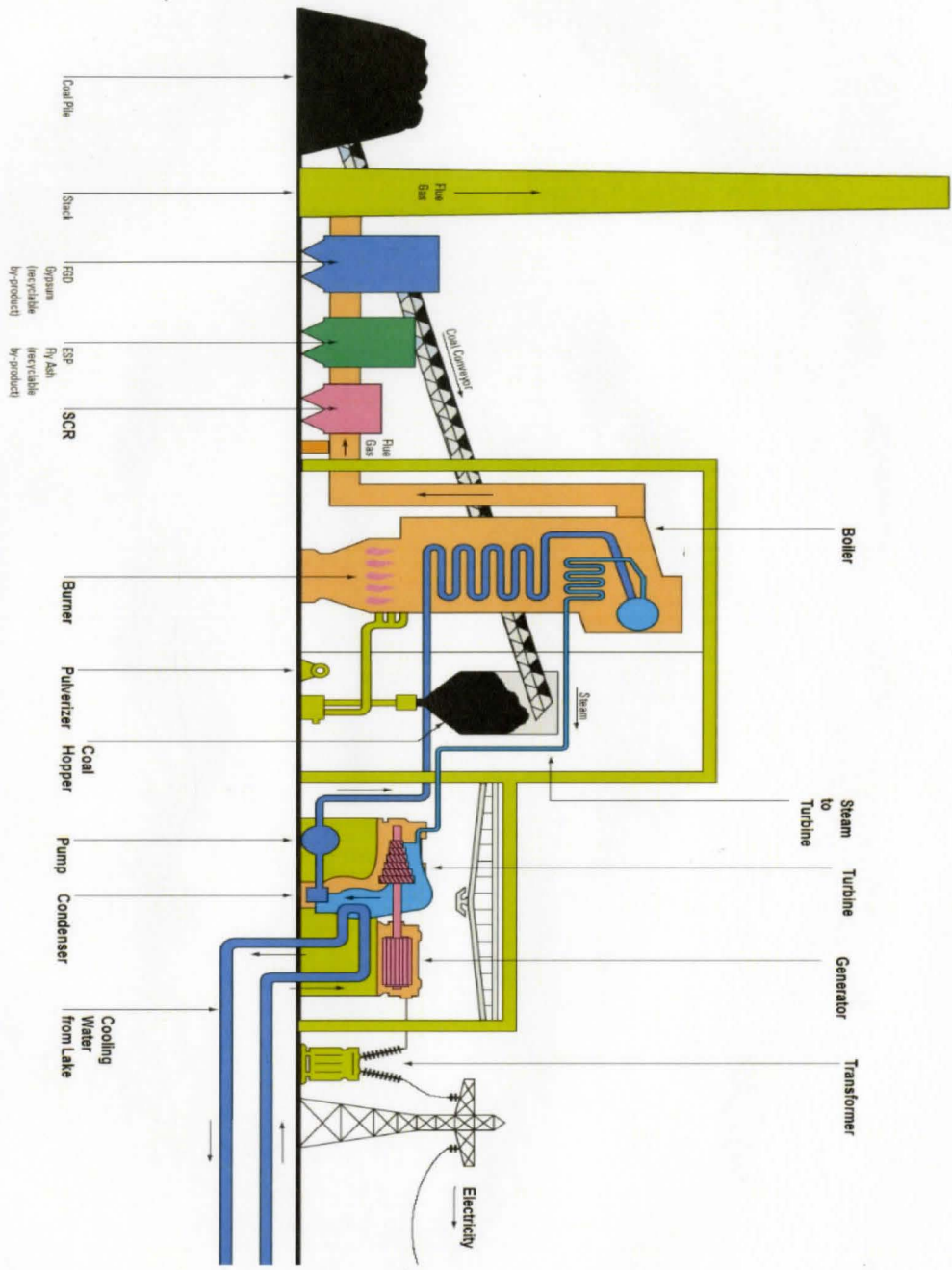This Appendix provides a diagram of a coal-fired generating plant : Ontario Power Generation's Atikokan Plant.

Figure B.1: Coal-fired generating plant diagram (Atikokan Generating Station [2008])

Appendix C

Pulp and Paper Mill Flow Sheet

This Appendix provides a flow sheet of a pulp and paper mill : created with the guidance of Don McCabe at Irving Pulp and Paper, Saint John, New Brunswick.
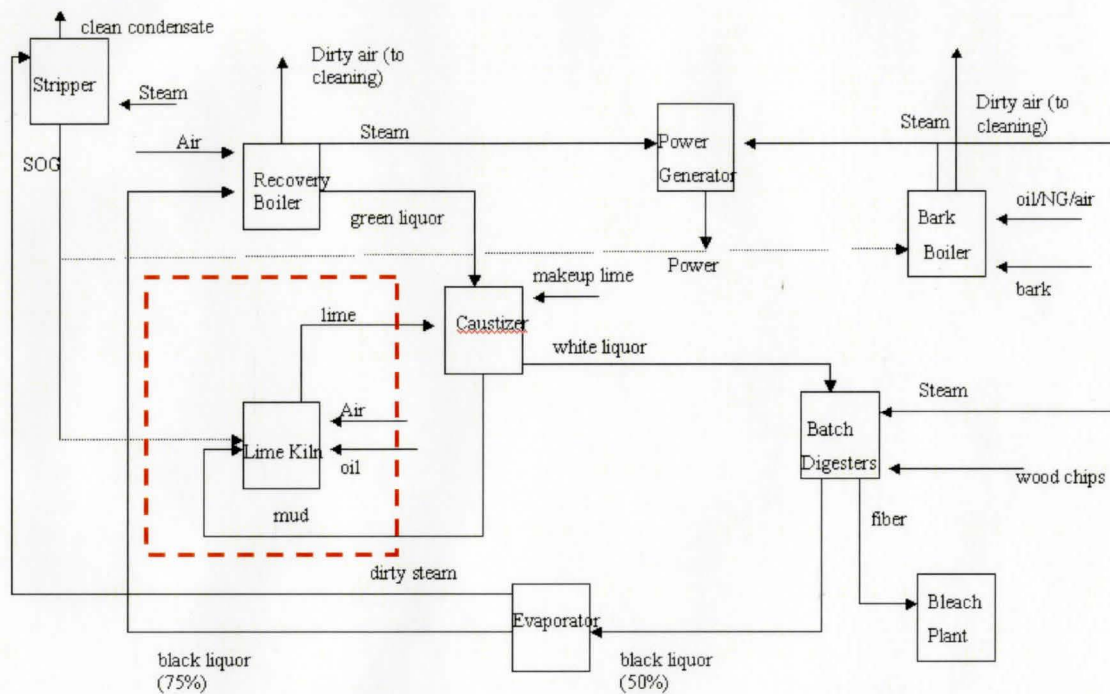
Figure C.1: Kraft Pulp and Paper Mill Flow Sheet